

Tunnelling spectroscopy of few-monolayer NbSe₂ in high magnetic field: triplet superconductivity and Ising protection

M. Kuzmanović,^{1,2,*} T. Dvir,^{3,4,†} D. LeBoeuf,⁵ S. Ilić,^{6,7} M. Haim,³ D.Möckli,^{3,8} S. Kramer,⁵ M. Khodas,³ M. Houzet,⁶ J. S. Meyer,⁶ M. Aprili,¹ H. Steinberg,³ and C. H. L. Quay¹

¹*Laboratoire de Physique des Solides (CNRS UMR 8502),
Bâtiment 510, Université Paris-Saclay 91405 Orsay, France*

²*QTF Centre of Excellence, Department of Applied Physics,
Aalto University School of Science,
P.O. Box 15100, 00076 Aalto, Finland*

³*Racah Institute of Physics, Hebrew University of Jerusalem,
Givat Ram, Jerusalem 91904 Israel*

⁴*QuTech and Kavli Institute of Nanoscience,
Delft University of Technology, 2600 GA Delft, the Netherlands*

⁵*Laboratoire National des Champs Magnétiques Intenses (LNCMI-EMFL),
CNRS, UGA, UPS, INSA, Grenoble/Toulouse, France*

⁶*Université Grenoble Alpes, CEA, Grenoble INP,
IRIG, PHELIQS, 38000 Grenoble, France*

⁷*Centro de Física de Materiales (CFM-MPC),
Centro Mixto CSIC-UPV/EHU, 20018 Donostia-San Sebastián, Spain*

⁸*Instituto de Física, Universidade Federal do Rio Grande do Sul,
91501-970 Porto Alegre, RS, Brazil*

Abstract

In conventional Bardeen-Cooper-Schrieffer (BCS) superconductors, Cooper pairs of electrons of opposite spin (i.e. singlet structure) form the ground state. Equal spin triplet pairs (ESTPs), as in superfluid ^3He , are of great interest for superconducting spintronics and topological superconductivity, yet remain elusive. Recently, odd-parity ESTPs were predicted to arise in (few-)monolayer superconducting NbSe_2 , from the non-collinearity between the out-of-plane Ising spin-orbit field (due to the lack of inversion symmetry in monolayer NbSe_2) and an applied in-plane magnetic field. These ESTPs couple to the singlet order parameter at finite field. Using van der Waals tunnel junctions, we perform spectroscopy of superconducting NbSe_2 flakes, of 2–25 monolayer thickness, measuring the quasiparticle density of states (DOS) as a function of applied in-plane magnetic field up to 33T. In flakes $\lesssim 15$ monolayers thick the DOS has a single superconducting gap. In these thin samples, the magnetic field acts primarily on the spin (vs orbital) degree of freedom of the electrons, and superconductivity is further protected by the Ising field. The superconducting energy gap, extracted from our tunnelling spectra, decreases as a function of the applied magnetic field. However, in bilayer NbSe_2 , close to the critical field (up to 30T, much larger than the Pauli limit), superconductivity appears to be more robust than expected from Ising protection alone. Our data can be explained by the above-mentioned ESTPs.

PACS numbers:

I. INTRODUCTION

In both superfluid ^3He and conventional Bardeen-Cooper-Schrieffer (BCS) superconductors, the ground state is made up of paired spinful entities, respectively nuclei and electrons. While the superfluid ^3He wavefunction has a spin triplet structure, conventional superconductors are spin singlet¹.

The question thus arises of the possible existence of triplet superconducting pairs, and in particular equal spin triplet pairs (ESTPs, linear combinations of $|\uparrow\uparrow\rangle$ and $|\downarrow\downarrow\rangle$), as have been found in $^3\text{He-A}^2$. ESTPs are intimately related to topological superconductivity and Majorana edge modes³. They are also of great interest for superconducting spintronics, as they can carry spin information without dissipation⁴.

ESTPs have recently been predicted to arise in (few-)monolayer superconducting 2H-NbSe₂ (hereafter NbSe₂) in an applied in-plane magnetic field⁵, as follows:

Monolayer transition metal dicalcogenides (TMDs), such as NbSe₂, with 2H structure lack in-plane crystal inversion symmetry; this gives rise, via the spin-orbit interaction, to an effective out-of-plane magnetic field H_{SO} known as the ‘Ising (spin-orbit) field’^{6–9}. H_{SO} is momentum-dependent; in particular, it has opposite sign at K and K’ points of the hexagonal Brillouin zone¹⁰, and a predicted amplitude¹¹ of $\mu_B H_{SO} = E_{SO} \approx 100$ meV in monolayer NbSe₂. As it is time-reversal invariant, H_{SO} does not affect the strength of singlet superconductivity; however, it causes Cooper pair spins to point out-of-plane (Figure 1(a)) — unlike conventional superconductors, where Cooper pairs’ internal spin axes have no preferred direction.

Thus, an applied in-plane magnetic field H_{\parallel} never completely aligns Cooper pair spins in the plane even when the Zeeman energy $E_Z = \mu_B H_{\parallel} \gg E_{SO}$: at zero temperature, the in-plane critical field H_c is expected to diverge logarithmically^{6,12}. In agreement with these expectations, TMD superconductors of (few-)monolayer thicknesses obtained by exfoliation¹³ or single-layer deposition^{14,15} show critical fields H_c much larger than $\mu_B H_P = \Delta_0/\sqrt{g}$, the Pauli or paramagnetic limit^{16,17,46}. (Here μ_B is the Bohr magneton, g the Landé g-factor and Δ_0 the superconducting order parameter at zero field.) While inversion symmetry is restored in even-layered NbSe₂, the enhancement of H_c persists in bilayer and few-monolayer TMDs, with H_c decreasing monotonically with increasing NbSe₂ thickness^{16,18,19}, and no observation of even-odd effects. This has been attributed to weak inter-layer coupling (compared to

$E_{SO})^{20}$ and/or spin-layer locking¹⁶.

Both singlet and opposite-spin triplet superconducting order parameters can exist at zero magnetic field, with spin structures respectively $\Phi_s = |\uparrow\downarrow\rangle - |\downarrow\uparrow\rangle$ and $\Phi_t = |\uparrow\downarrow\rangle + |\downarrow\uparrow\rangle$ ²¹. For $E_{SO} < E_F$ (the Fermi energy), which is the case here, Φ_t and Φ_s decouple, and Φ_t should not coexist with Φ_s ^{22,23}. (Φ_t is in any case sensitive to disorder and disappears when the mean free path is shorter than the superconducting coherence length⁵.)

The applied in-plane field $H_{||}$, due to its non-collinearity with the Ising field, as well as the momentum dependence of the latter, results in ESTPs with spin structure $\Phi_{tB} = |\downarrow\downarrow\rangle + |\uparrow\uparrow\rangle$ ^{5,24,25} (Figure 1(b)). Φ_{tB} is coupled to Φ_s by the in-plane field, and the critical field is affected by their symbiotic relationship²⁶: Φ_{tB} enables Φ_s to survive the magnetic field, while Φ_s enables Φ_{tB} to survive disorder. As a result, in a disordered sample, or even when the temperature $T > T_{ct}$ (the critical temperature associated with Φ_{tB}), the in-plane critical field is higher than it would be for either Φ_s or Φ_{tB} alone, and the dependence of the superconducting gap Δ on the applied field is also affected (Figure 1(c)).

Very recently, a two-fold anisotropy of critical field, non-linear transport and magnetoresistance was observed in few- and mono-layer NbSe₂ devices close to the transition to the normal state^{27,28}. These results were also interpreted as coming from unconventional superconductivity: Φ_{tB} triplet components induced by the applied magnetic field and lateral lattice strain can reduce the six-fold rotational symmetry expected from the hexagonal crystal lattice to two-fold symmetry²⁷⁻²⁹.

Here we report tunnelling spectroscopy of few-monolayer NbSe₂ devices over a wide range of applied in-plane magnetic fields, up to 30 T. As the magnetic field increases, our measurement of the superconducting gap Δ progressively deviates from the prediction based on pure singlet pairing. We find that this field-induced deviation can be explained by the onset of ESTPs in the form of Φ_{tB} (Figure 1).

II. RESULTS

We consider a single-band superconductor, with hole pockets at the K/K' points, and include Φ_s and Φ_{tB} correlations. As mentioned above, Φ_{tB} is coupled linearly to Φ_s , and is expressed even when $\Delta_{tB} < \Delta_s$. If we neglect inter-valley scattering, and if a finite pairing interaction is present in the Φ_{tB} channel as suggested by recent density functional

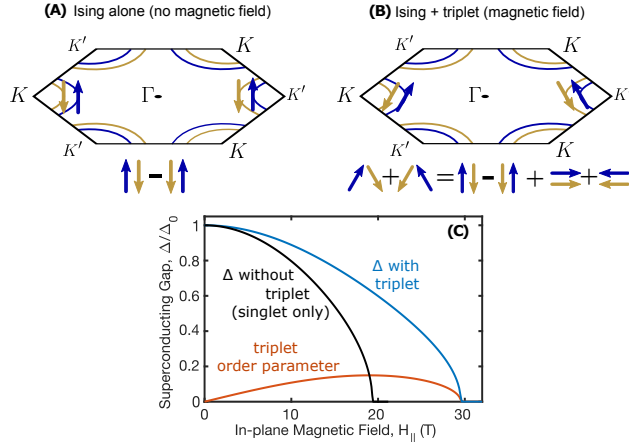


FIG. 1: (a) At zero magnetic field, singlet Cooper pairs are composed of electrons at opposite corners of the hexagonal NbSe₂ Brillouin zone (K and K' points). Their spins are pinned out-of-plane by the Ising field. (b) An in-plane magnetic field partially aligns electron spins orthogonal to the Ising field, and gives rise to odd-parity equal-spin triplet pairs⁵. (c) Theoretical superconducting gap as a function of in-plane magnetic field. Compared to the case where only the Ising field is considered (black line), superconductivity is even more robust to the in-plane magnetic field and the Δ vs $H_{||}$ curve has a ‘flattened’ shape at intermediate fields (blue line). The triplet component of the order parameter (red line) with spin structure Φ_{tB} survives disorder through its coupling to the singlet component, which has spin structure Φ_s . The temperature used in the calculations is $0.5 T_c$, the critical temperature. See Figure 4 and the text for details and comparison to data.

theory (DFT) calculations¹¹, the superconducting energy gap Δ can be obtained from the quasiclassical theory of superconductivity (cf. Equation S14 in Supp. Info.) :

$$\Delta = (E_{SO}\Delta_s + E_Z\Delta_{tB})/\sqrt{E_{SO}^2 + E_Z^2}, \quad (1)$$

where Δ_s and Δ_{tB} are, respectively, the singlet and equal-spin triplet order parameters.

Here we can see that, compared to the case of Φ_s with Ising protection alone, the co-existence of Δ_{tB} with Δ_s and the coupling between the two can increase the robustness of superconductivity against an applied in-plane magnetic field. In the case where there is no pairing in the equal-spin triplet channel ($\Delta_{tB} = 0$), Δ is reduced by the magnetic field through the factor $E_{SO}/\sqrt{E_{SO}^2 + E_Z^2}$ and vanishes asymptotically, giving the aforementioned logarithmic divergence of the critical field at zero temperature. To obtain the

order parameters Δ_s and Δ_{tB} at finite temperature and magnetic field, one has to solve two coupled equations self-consistently (cf. Supp. Info. II).

The quasiclassical theory also gives the density of states (DOS), which is found for $E < E_{SO}$ to be simply the BCS DOS, with the gap as in Equation 1 (see Equation 14 in the Supp. Info.) — unlike 2D superconductors with low spin-orbit coupling in in-plane fields, the coherence peak is not Zeeman-split³⁰. In addition, Ising protection gives a sharp coherence peak in the DOS, regardless of the strength of the triplet coupling or the applied magnetic field. Nevertheless, in the presence of inter-valley scattering (τ_{iv} being the inter-valley scattering time), Ising protection is reduced (due to averaging over valleys with opposite signs of H_{SO}), the DOS is smeared out²³ as in the Abrikosov-Gor'kov theory^{31,32}, and the divergence of the critical field at zero temperature is regularised¹². In the limit of strong inter-valley scattering ($E_{SO}^2/\Delta_s \gg 1/\tau_{iv} \gg \Delta_0$) the dependence of Δ on the applied magnetic field becomes similar to that expected from the Abrikosov-Gor'kov theory with the critical field given by $\mu_B H_c = E_{SO} \sqrt{2\Delta\tau_{iv}/\hbar}$. In our experiment, we do not have strong inter-valley scattering as $1/\tau_{iv} \lesssim \Delta_s$. (See Supp. Info. IC)

We fabricate tunnel junctions (J1 to J7) on superconducting NbSe₂ flakes of 1.2 – 50 nm thickness. The tunnel barriers are thin flakes of semiconducting WSe₂ or MoS₂ exfoliated by the van der Waals dry transfer technique described in Ref.³³. A Ti/Au normal counter electrode is then evaporated on the semiconductor leading to a structure shown schematically in Figure 2(a). An ohmic contact to the NbSe₂ is also fabricated. The typical surface area of the junction is about 1 μm^2 and the resistance in the normal state >10 k Ω . The critical temperature T_c decreases from ~ 7.2 K in the thickest flakes to ~ 2.6 K in the thinnest ones.

Using standard lock-in techniques, we first measure the current I and differential conductance $G = dI/dV$ across the junctions as a function of applied bias voltage V ³⁴ and in-plane magnetic fields H_{\parallel} in dilution refrigerators with base temperatures of 30–70 mK. $G(V)$ is proportional to the DOS convolved with the derivative of the Fermi distribution function³⁵. Therefore, in principle, the energy resolution of our spectroscopy is given by the temperature and the integrated voltage noise across the junction.

Typical $G(V)$ curves are shown for a 25 nm thick sample (J2) and a 6 monolayer sample (J6) in Figure 2(b,c), top panels. The main differences between these junctions are: (1) the smaller superconducting gap in the thinner device due to a smaller T_c , and (2) the low-energy shoulder, very clearly seen in the thicker junction, is absent in the thinner one. This is even

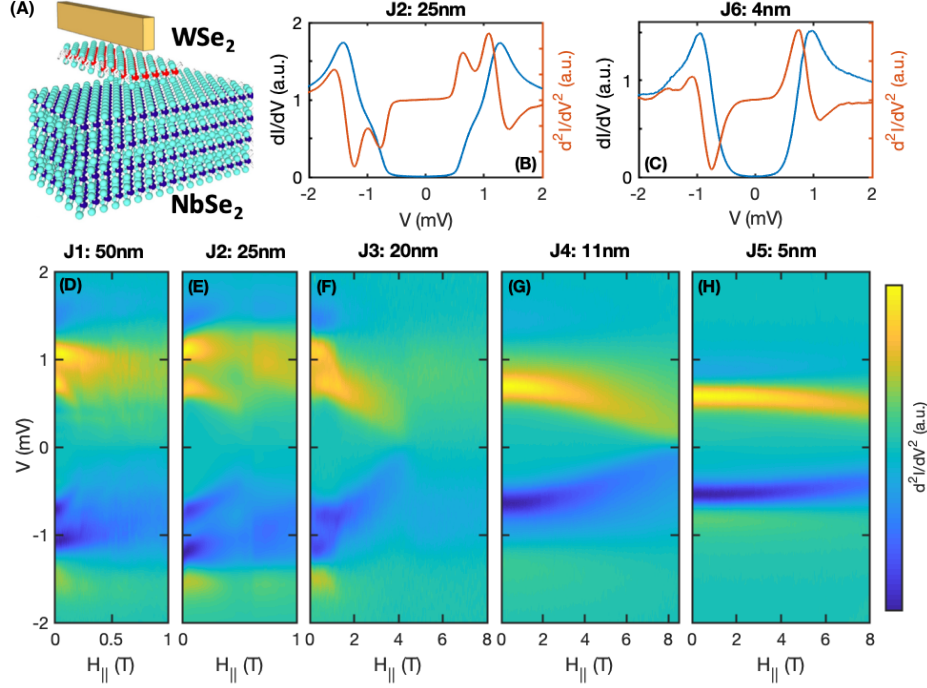


FIG. 2: Tunnelling spectroscopy of bulk and few-monolayer NbSe₂ through van der Waals barriers. (a) Schematic drawing of the tunnel junction: few-monolayer NbSe₂, covered with few-monolayer WSe₂ (or MoS₂) and a Ti/Au electrode. A voltage V is applied between the Ti/Au electrode and the NbSe₂ and a current I measured. (b) Differential conductance ($G = dI/dV$) as a function of V across J2 (blue) and d^2I/dV^2 vs V of J2 (red). A double peak/dip can be seen in d^2I/dV^2 , due to the presence of two superconducting gaps. (c) Same as panel (b) for J6. (d)-(h) Colormaps of the magnetic field dependence of the d^2I/dV^2 curves for junctions J1–J5. The double dip/peak feature (yellow/blue regions) disappears in thin samples; a single gap is left. Measurements were taken at temperatures of 30-70 mK.

more apparent in the second derivative of the current as a function of the voltage bias, dG/dV , in Figure 2(b,c): the two peaks in J2, merge to a single peak in J6. This merging was previously observed^{33,36} and we now see that it persists in flakes up to 11 nm (≈ 15 monolayer) thick: the two-gap superconductivity of bulk NbSe₂³⁷ is lost. This is consistent with band structure calculations for bulk and monolayer NbSe₂: whereas in the bulk three bands cross the Fermi level^{38,39}, and two superconducting gaps have been observed³³, in the monolayer a single band remains, which crosses the Fermi level twice, resulting in hole pockets at the K/K' and Γ points¹¹. A single-band theory thus seems most suitable for the

thinnest flakes.

Figures 2(d-h) show the evolution of the dG/dV curves of five junctions (J1-J5) with increasing in-plane magnetic field. Junctions 1 and 2, the thickest, show similar responses to the applied field: the inner peak shifts to lower energies faster than the outer peak. This is consistent with previous experiments, and is likely due to the 3D character of the Se p_z -orbital-derived band at the Γ point, which is associated with the smaller superconducting energy gap, as well as its higher diffusion coefficient^{33,40}. For the thinner junctions, J4 and J5, a single gap persists from zero field up to 9 T.

As noted above, the robustness of the gap to applied magnetic fields is expected in thin samples due to Ising protection and drastically reduced orbital depairing (Meissner effect). To significantly reduce the gap and to study the effect of the applied field on the density of states it is necessary to go to even higher fields.

Therefore, we measure two tunnel junctions (J6, 6 monolayers) and (J7, bilayer) in in-plane magnetic fields of up to 33 T at 1.3 K (pumped liquid helium). Their critical temperatures are, respectively, 5.4 K ($H_P = 10.5$ T) and 2.6 K ($H_P = 5$ T), giving $\Delta/k_B T_c \approx 1.8$, close to the BCS prediction and in agreement with previous studies^{33,36}. (See Figure S2 and inset.) Finally, the critical in-plane fields are $H_c = 18$ T for J6 and $H_c = 30$ T for J7, corresponding respectively to $H_c = 1.5H_P$ and $H_c = 6H_P$. (See Figure 4.) These junctions had earlier been characterized at 50mK (dilution refrigerator) at zero magnetic field (Figures 3(c) and (f)) — hard gaps were observed, pointing to tunnelling as the main transport mechanism. These tunnel spectra are well-described by a fit to a BCS density of states, broadened by a $\sim 200\mu eV$ effective temperature. Though higher than the bath temperature, this broadening does not affect the determination of the energy gap, which can be done with high precision. (See Supp. Info. IA and IB for details.)

III. DISCUSSION

The evolution of $G(V)$ with the in-plane magnetic field at 1.3K is shown in Figures 3(a) (J6) and 3(d) (J7). For clarity, spectra at selected magnetic fields are also shown in Figures 3(b) and 2(e) together with an Abrikosov-Gor'kov-like density of states with a field-dependent broadening parameter^{31,41}, convolved with a Fermi function to account for the temperature. The fits account very well for the experimental data.

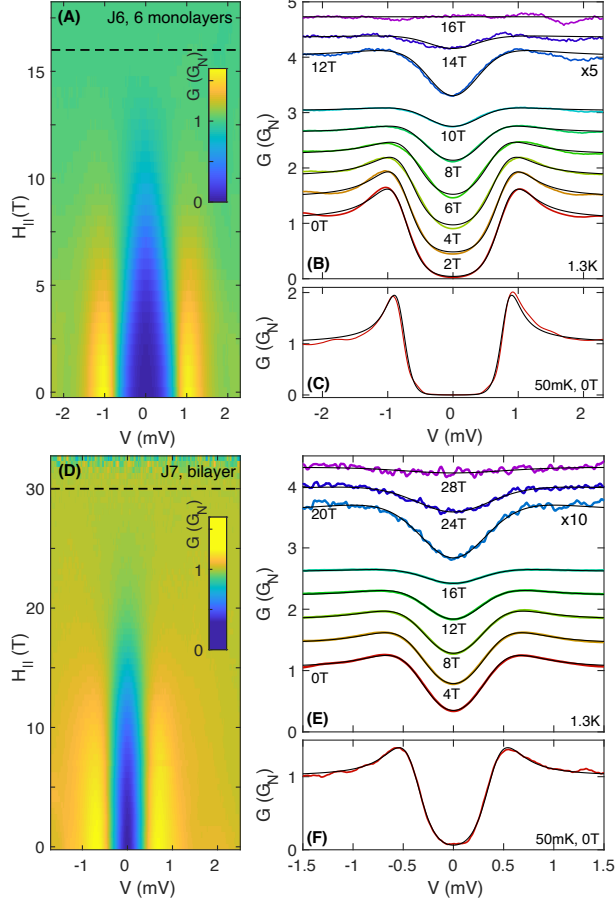


FIG. 3: Differential conductance $G = dI/dV$ as a function of the bias voltage V and of the in-plane magnetic field H_{\parallel} of J6 (6 monolayers, top panels) and J7 (bilayer, bottom panels). The tunnelling spectra are normalized by the normal state conductance, $G_N(V)$, measured above H_c . (a,d) Colormap of $G(V)$ as a function of field at 1.3 K. The dotted lines indicate the critical fields. (b,e) Horizontal slices of the data in the colormaps (a) and (d) respectively, showing $G(V)$ at different fields, vertically displaced for clarity. The black lines are fits to an Abrikosov-Gor'kov-like (A-G-like) density of states, with the energy gap and A-G broadening parameter as fitting parameters. (The gap is not determined self-consistently.) (c,f) Data at 50mK and zero magnetic field (red lines) together with the fits obtained using a BCS DOS and an effective temperature (black lines). The superconducting gaps obtained from the fits are, respectively, $800\mu\text{eV}$ and $400\mu\text{eV}$, while the effective temperatures are respectively 0.9K and 1K.

The superconducting gaps obtained from these fits are shown as a function of the in-plane magnetic field in Figure 4, and compared to theory.

For the six-monolayer device, a simple Ising model accounts for the data reasonably well (Figure 4, dashed dark blue line). The fitting parameters are given in the caption of the figure.

Focusing on the thinner, bilayer device (J7), we see that the Ising theory alone without triplet pairing fits the data reasonably well up to about 20T, but not close to the critical field, where the superconducting energy gap is more robust than expected (Figure 4, dashed dark blue line).

This key experimental finding is suggestive of a second order parameter, which is revealed as the dominant order parameter disappears²². Indeed introducing a small ESTP component of the gap (triplet model), a better fit of the overall experimental data is obtained (Figure 4, brown line). The temperature of the experiment (1.3K) is above the triplet critical temperature ($T_{ct} = 0.05T_{cs} = 130\text{mK}$, obtained from the fit). Therefore, the ESTP order parameter Δ_{tB} exists only through its coupling with the singlet order parameter Δ_s , and its main effect is to enhance the critical field through the coupling with the singlet order parameter. In addition, the triplet subdominant component also renders the gap vs field dependence more linear (Figure 1(c)).

Our fit also gives $E_{SO} = 9.62T_{cs}$ (~ 2.2 meV). This is a lower bound for E_{SO} , as inter-valley (K-K') scattering is not taken into account. If it is, higher values of E_{SO} will have to be used to arrive at the same $H_{||}^c$, but the shape of the $\Delta(H_{||})$ curve is similar. Further, we note that the shape of $\Delta(H_{||})$ in the triplet model is by construction impervious to intra-valley scattering. Our E_{SO} value is consistent with the upper bound for E_{SO} given by angle-resolved photo-emission spectroscopy (ARPES) measurements, which indicate $E_{SO} \lesssim 20\text{meV}$ (the measurement resolution), significantly lower than theoretical predictions⁴².

For completeness, we also show the Ising theory with strong inter-valley scattering (equivalent to Abrikosov-Gor'kov), where the only fitting parameter is the critical field (Figure 4, black line). This does not fit the data at all – the experimental Δ is consistently smaller than that predicted by the theory, which also fails to reproduce the ‘linear’ part of the curve at intermediate fields.

At present, much of the literature on quantum transport in few-layer NbSe₂ includes only the hole pockets at the K/K' points, as we did, even though there is also a hole pocket at the Γ point¹¹. In Supp. Info. IIC and IID, we consider models which include only Φ_s and K/K'- Γ coupling, and neglect all triplet order parameters. These are found not to fit our

data well, given the known level of disorder in the sample, thus strengthening the case for the ESTP interpretation.

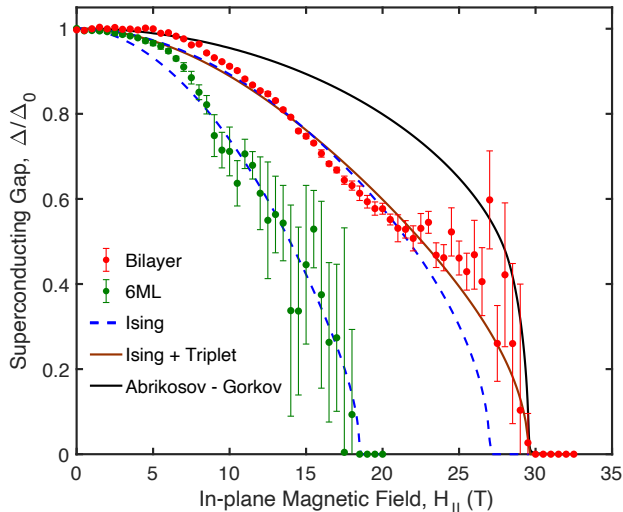


FIG. 4: Normalized superconducting gap as a function of the in-plane magnetic field $\Delta(H_{\parallel})$ obtained from the fits of the quasiparticle density of states in Figure 3. The error bars were obtained following the procedure described in Supp. Info. IA. The dark blue dashed lines are a fit of experimental data using the Ising theory alone. Here, $E_{SO} = 14.45T_{cs}$ (with $T_{cs} = 2.6K$) for the bilayer and $E_{SO} = 2.21T_{cs}$ (with $T_{cs} = 5.4K$) for the 6-monolayer. In brown is the Ising theory with an equal-spin triplet component of the order parameter as described in the text. Here, $E_{SO} = 9.62T_{cs}$ and $T_{ct} = 0.05T_{cs}$, with $T_{cs} = 2.6K$. Finally, the solid black line is calculated using the Ising theory with strong disorder (equivalent to the Abrikosov-Gor'kov theory). In all cases, the critical field is constrained to be the experimental one.

Regarding ESTPs, we note that, within the scenarios of Refs.^{27,28} mentioned earlier, the triplet order parameters allowed by symmetry such as Φ_{tB} have to be nearly degenerate with the leading singlet order parameter. Attraction in the triplet channel is supported by recent density functional theory (DFT) calculations¹¹; however, there is at present no evidence of near degeneracy between triplet and singlet channels. Our interpretation does not require near degeneracy, and the singlet-triplet coupling comes from a clear microscopic mechanism (the in-plane magnetic field), which is quantitatively accounted for both in the theory and in the analysis of the experimental data.

While previous reports on Andreev spectroscopy experiments have shown a reduction of the gap consistent with field-induced depairing in the presence of Ising protection⁴³, our hard-

gap tunnel junctions allow a nuanced and quantitative analysis of the possible microscopic mechanisms for the enhancement of the critical field, pointing to the presence of equal-spin triplet superconductivity.

Further study at even lower temperatures, independent measurements of E_{SO} , independent estimates of the K/K'- Γ coupling from theory or experiment, and momentum-selective barriers would be helpful to unambiguously confirm the existence of ESTPs in NbSe₂.

IV. MATERIALS AND METHODS

Especially at high magnetic fields, special care was taken to ensure that the applied magnetic field is parallel to the flakes. It is aligned to better than $\sim 1^\circ$. In addition, we checked that the voltage noise due to mechanical vibrations is lower than that from the thermal broadening. This is described in detail in Supp. Info. IA.

V. DATA AVAILABILITY

The datasets generated and/or analysed during the current study are available from the corresponding author upon reasonable request.

VI. ACKNOWLEDGEMENTS

We acknowledge valuable discussions with Pascal Simon and Freek Masee, and thank the latter for a careful reading of the manuscript. This work was funded by a Maimonides-Israel grant from the Israeli-French High Council for Scientific and Technological Research; JCJC (SPINOES), PIRE (HYBRID) and PRC (TRIPRES) grants from the French Agence Nationale de Recherche; ERC Starting Grant ERC-2014-STG 637928 (TUNNEL); Israel Science Foundation Grants No.s 861/19 and 2665/20, and the Laboratoire d'Excellence LANEF in Grenoble (ANR10-LABX-51-01). T.D. is grateful to the Azrieli Foundation for an Azrieli Fellowship. Part of this work has been performed at the Laboratoire National de Champs Magnétiques Intenses (LNCMI), a member of the European Magnetic Field

Laboratry (EMFL).

- * These two authors contributed equally.
- † These two authors contributed equally
- ¹ Annett, J. F. Superconductivity, Superfluids, and Condensates (Oxford University Press, Oxford ; New York, 2004), 1st edition edn.
- ² Leggett, A. J. Nobel Lecture: Superfluid $^3\mathrm{He}$: the early days as seen by a theorist*. Reviews of Modern Physics **76**, 999–1011 (2004). URL <http://link.aps.org/doi/10.1103/RevModPhys.76.999>.
- ³ Frolov, S. M., Manfra, M. J. & Sau, J. D. Topological superconductivity in hybrid devices. Nature Physics **16**, 718–724 (2020). URL <https://www.nature.com/articles/s41567-020-0925-6>.
- ⁴ Ohnishi, K. et al. Spin-transport in superconductors. Applied Physics Letters **116**, 130501 (2020). URL <http://aip.scitation.org/doi/10.1063/1.5138905>.
- ⁵ Möckli, D. & Khodas, M. Ising superconductors: Interplay of magnetic field, triplet channels, and disorder. Physical Review B **101**, 014510 (2020). URL <https://link.aps.org/doi/10.1103/PhysRevB.101.014510>.
- ⁶ Frigeri, P. A., Agterberg, D. F. & Sigrist, M. Spin susceptibility in superconductors without inversion symmetry. New Journal of Physics **6**, 115 (2004). URL <http://iopscience.iop.org/article/10.1088/1367-2630/6/1/115/meta>. Publisher: IOP Publishing.
- ⁷ Gor’kov, L. P. & Rashba, E. I. Superconducting 2D System with Lifted Spin Degeneracy: Mixed Singlet-Triplet State. Physical Review Letters **87**, 037004 (2001). URL <https://link.aps.org/doi/10.1103/PhysRevLett.87.037004>. Publisher: American Physical Society.
- ⁸ Saito, Y. et al. Superconductivity protected by spin–valley locking in ion-gated MoS₂. Nature Physics **12**, 144–149 (2016). URL <https://www.nature.com/articles/nphys3580>.
- ⁹ Lu, J. M. et al. Evidence for two-dimensional Ising superconductivity in gated MoS₂. Science **350**, 1353–1357 (2015). URL <https://science.sciencemag.org/content/350/6266/1353>.
- ¹⁰ Xu, X., Yao, W., Xiao, D. & Heinz, T. F. Spin and pseudospins in layered transition metal dichalcogenides. Nature Physics **10**, 343–350 (2014). URL <https://www.nature.com/articles/nphys2942>. Number: 5 Publisher: Nature Publishing Group.

- ¹¹ Wickramaratne, D., Khmelevskiy, S., Agterberg, D. F. & Mazin, I. Ising Superconductivity and Magnetism in NbSe_2 . Physical Review X **10**, 041003 (2020). URL <https://link.aps.org/doi/10.1103/PhysRevX.10.041003>.
- ¹² Ilić, S., Meyer, J. S. & Houzet, M. Enhancement of the Upper Critical Field in Disordered Transition Metal Dichalcogenide Monolayers. Physical Review Letters **119**, 117001 (2017). URL <https://link.aps.org/doi/10.1103/PhysRevLett.119.117001>. Publisher: American Physical Society.
- ¹³ Wang, Q. H., Kalantar-Zadeh, K., Kis, A., Coleman, J. N. & Strano, M. S. Electronics and optoelectronics of two-dimensional transition metal dichalcogenides. Nature Nanotechnology **7**, 699–712 (2012). URL <https://www.nature.com/articles/nnano.2012.193>. Number: 11 Publisher: Nature Publishing Group.
- ¹⁴ Zhang, T. et al. Superconductivity in one-atomic-layer metal films grown on Si(111). Nature Physics **6**, 104–108 (2010). URL <https://www.nature.com/articles/nphys1499>. Number: 2 Publisher: Nature Publishing Group.
- ¹⁵ Fan, Q. et al. Plain s-wave superconductivity in single-layer FeSe on SrTiO₃ probed by scanning tunnelling microscopy. Nature Physics **11**, 946–952 (2015). URL <https://www.nature.com/articles/nphys3450>. Number: 11 Publisher: Nature Publishing Group.
- ¹⁶ Xi, X. et al. Ising pairing in superconducting NbSe₂ atomic layers. Nature Physics **12**, 139–143 (2016). URL <https://www.nature.com/articles/nphys3538>. Number: 2 Publisher: Nature Publishing Group.
- ¹⁷ Liu, Y. et al. Interface-Induced Zeeman-Protected Superconductivity in Ultrathin Crystalline Lead Films. Physical Review X **8**, 021002 (2018). URL <https://link.aps.org/doi/10.1103/PhysRevX.8.021002>. Publisher: American Physical Society.
- ¹⁸ de la Barrera, S. C. et al. Tuning Ising superconductivity with layer and spin–orbit coupling in two-dimensional transition-metal dichalcogenides. Nature Communications **9**, 1427 (2018). URL <https://www.nature.com/articles/s41467-018-03888-4>. Number: 1 Publisher: Nature Publishing Group.
- ¹⁹ Prober, D. E., Schwall, R. E. & Beasley, M. R. Upper critical fields and reduced dimensionality of the superconducting layered compounds. Physical Review B **21**, 2717–2733 (1980). URL <https://link.aps.org/doi/10.1103/PhysRevB.21.2717>. Publisher: American Physical Society.
- ²⁰ Jones, A. M. et al. Spin–layer locking effects in optical orientation of exciton spin in bilayer WSe₂

2. *Nature Physics* **10**, 130–134 (2014). URL <https://www.nature.com/articles/nphys2848>.
Number: 2 Publisher: Nature Publishing Group.
- ²¹ Smidman, M., Salamon, M. B., Yuan, H. Q. & Agterberg, D. F. Superconductivity and spin–orbit coupling in non-centrosymmetric materials: a review. *Reports on Progress in Physics* **80**, 036501 (2017). URL <https://doi.org/10.1088/1361-6633/80/3/036501>.
- ²² Rainer, D., Burkhardt, H., Fogelström, M. & Sauls, J. A. Andreev bound states, surfaces and subdominant pairing in high T_c superconductors. *Journal of Physics and Chemistry of Solids* **59**, 2040–2044 (1998). URL <https://www.sciencedirect.com/science/article/pii/S0022369798001759>.
- ²³ Haim, M., Möckli, D. & Khodas, M. Signatures of triplet correlations in density of states of Ising superconductors. *Phys. Rev. B* **102**, 214513 (2020). URL <https://link.aps.org/doi/10.1103/PhysRevB.102.214513>.
- ²⁴ Tang, G., Bruder, C. & Belzig, W. Magnetic field-induced "mirage" gap in an Ising superconductor. *arXiv:2011.07080 [cond-mat]* (2020). URL <http://arxiv.org/abs/2011.07080>. ArXiv: 2011.07080.
- ²⁵ Nakamura, Y. & Yanase, Y. Odd-parity superconductivity in bilayer transition metal dichalcogenides. *Physical Review B* **96**, 054501 (2017). URL <https://link.aps.org/doi/10.1103/PhysRevB.96.054501>. Publisher: American Physical Society.
- ²⁶ Möckli, D. & Khodas, M. Magnetic-field induced s_+ pairing in Ising superconductors. *Physical Review B* **99**, 180505 (2019). URL <https://link.aps.org/doi/10.1103/PhysRevB.99.180505>.
- ²⁷ Hamill, A. *et al.* Unexpected two-fold symmetric superconductivity in few-layer nbse₂. *arXiv:2004.02999* (2020). URL <https://arxiv.org/abs/2004.02999>. ArXiv: 2004.02999.
- ²⁸ Cho, C.-W. *et al.* Distinct nodal and nematic superconducting phases in the 2D Ising superconductor NbSe₂. *arxiv:2003.12467* (2020).
- ²⁹ Haim, M., Levchenko, A. & Khodas, M. Mechanisms of in-plane magnetic anisotropy in superconducting NbSe_2 . *Physical Review B* **105**, 024515 (2022). URL <https://link.aps.org/doi/10.1103/PhysRevB.105.024515>.
- ³⁰ Meservey, R., Tedrow, P. M. & Fulde, P. Magnetic Field Splitting of the Quasiparticle States in Superconducting Aluminum Films. *Physical Review Letters* **25**, 1270–1272 (1970). URL <http://link.aps.org/doi/10.1103/PhysRevLett.25.1270>.

- ³¹ Abrikosov, A. A. & Gor'kov, L. P. Contribution to the theory of superconducting alloys with paramagnetic impurities. JETP **12**, 1243 (1961).
- ³² Bruno, R. C. & Schwartz, B. B. Magnetic Field Splitting of the Density of States of Thin Superconductors. Physical Review B **8**, 3161–3178 (1973). URL <https://link.aps.org/doi/10.1103/PhysRevB.8.3161>.
- ³³ Dvir, T. et al. Spectroscopy of bulk and few-layer superconducting NbSe₂ with van der Waals tunnel junctions. Nature Communications **9**, 598 (2018). URL <https://www.nature.com/articles/s41467-018-03000-w>. Number: 1 Publisher: Nature Publishing Group.
- ³⁴ Giaever, I. Energy Gap in Superconductors Measured by Electron Tunneling. Physical Review Letters **5**, 147–148 (1960). URL <https://link.aps.org/doi/10.1103/PhysRevLett.5.147>. Publisher: American Physical Society.
- ³⁵ Tinkham, M. Introduction to Superconductivity (Dover, Mineola, 1996), 2 edn.
- ³⁶ Khestanova, E. et al. Unusual Suppression of the Superconducting Energy Gap and Critical Temperature in Atomically Thin NbSe₂. Nano Letters **18**, 2623–2629 (2018). URL <https://doi.org/10.1021/acs.nanolett.8b00443>. Publisher: American Chemical Society.
- ³⁷ Noat, Y. et al. Quasiparticle spectra of $2H\text{-NbSe}_2$: Two-band superconductivity and the role of tunneling selectivity. Physical Review B **92**, 134510 (2015). URL <https://link.aps.org/doi/10.1103/PhysRevB.92.134510>. Publisher: American Physical Society.
- ³⁸ Johannes, M. D., Mazin, I. I. & Howells, C. A. Fermi-surface nesting and the origin of the charge-density wave in NbSe_2 . Physical Review B **73**, 205102 (2006). URL <https://link.aps.org/doi/10.1103/PhysRevB.73.205102>. Publisher: American Physical Society.
- ³⁹ Yokoya, T. et al. Fermi Surface Sheet-Dependent Superconductivity in $2H\text{-NbSe}_2$. Science (2001). URL <https://www.science.org/doi/abs/10.1126/science.1065068>. Publisher: American Association for the Advancement of Science.
- ⁴⁰ Dvir, T., Aprili, M., Quay, C. H. L. & Steinberg, H. Tunneling into the Vortex State of NbSe₂ with van der Waals Junctions. Nano Letters **18**, 7845–7850 (2018). URL <https://doi.org/10.1021/acs.nanolett.8b03605>. Publisher: American Chemical Society.
- ⁴¹ Srivastava, R. V. A. & Teizer, W. Analytical density of states in the Abrikosov-Gorkov theory. Solid State Communications **145**, 512–513 (2008). URL <https://www.sciencedirect.com/>

science/article/pii/S0038109807008344.

- ⁴² Xu, C.-Z. et al. Experimental and theoretical electronic structure and symmetry effects in ultrathin $\{\mathrm{NbSe}\}_2$ films. Physical Review Materials **2**, 064002 (2018). Publisher: American Physical Society.
- ⁴³ Sohn, E. et al. An unusual continuous paramagnetic-limited superconducting phase transition in 2D NbSe 2. Nature Materials **17**, 504–508 (2018). URL <https://www.nature.com/articles/s41563-018-0061-1>. Number: 6 Publisher: Nature Publishing Group.
- ⁴⁴ Clogston, A. M. Upper Limit for the Critical Field in Hard Superconductors. Physical Review Letters **9**, 266–267 (1962). URL <https://link.aps.org/doi/10.1103/PhysRevLett.9.266>. Publisher: American Physical Society.
- ⁴⁵ Fulde, P. High field superconductivity in thin films. Advances in Physics **22**, 667–719 (1973). URL <http://www.tandfonline.com/doi/abs/10.1080/00018737300101369>.
- ⁴⁶ At the Pauli limit, the paramagnetic state of spin-aligned quasiparticles becomes more energetically favourable than the superconducting ground state^{44,45}. In the absence of spin-orbit coupling, H_P is thus the expected H_c for thin superconductors, where the Meissner effect can be neglected.

SUPPLEMENTAL MATERIAL for

“Tunnelling spectroscopy of few-monolayer NbSe₂ in high magnetic field: triplet superconductivity and Ising protection”

M. Kuzmanović,^{1,2,*} T. Dvir,^{3,4,*} D. LeBoeuf,⁵ S. Ilić,^{6,7} M. Haim,³ D.Möckli,^{3,8} S. Kramer,⁵
M. Khodas,³ M. Houzet,⁶ J. S. Meyer,⁶ M. Aprili,¹ H. Steinberg,³ and C. H. L. Quay¹

¹*Laboratoire de Physique des Solides (CNRS UMR 8502),
Bâtiment 510, Université Paris-Saclay 91405 Orsay, France*

²*QTF Centre of Excellence, Department of Applied Physics,*

Aalto University School of Science, P.O. Box 15100, 00076 Aalto, Finland

³*Racah Institute of Physics, Hebrew University of Jerusalem, Givat Ram, Jerusalem 91904 Israel*

⁴*QuTech and Kavli Institute of Nanoscience, Delft University of Technology, 2600 GA Delft, the Netherlands*

⁵*Laboratoire National des Champs Magnétiques Intenses (LNCMI-EMFL),
CNRS, UGA, UPS, INSA, Grenoble/Toulouse, France*

⁶*Université Grenoble Alpes, CEA, Grenoble INP, IRIG, PHELIQS, 38000 Grenoble, France*

⁷*Centro de Física de Materiales (CFM-MPC), Centro Mixto CSIC-UPV/EHU, 20018 Donostia-San Sebastián, Spain*

⁸*Instituto de Física, Universidade Federal do Rio Grande do Sul, 91501-970 Porto Alegre, RS, Brazil*

PACS numbers:

The supplementary material is divided into two parts. Part **I** covers the experimental methods: section **IA** details how the order parameter was extracted from the spectroscopic data and gives an estimate of the uncertainty, while sections **IB** and **IC** comment on the broadening of the density of states and the disorder respectively. Part **II** presents the details of the theoretical model, where a general overview is given in section **IIA**, followed by the triplet model in section **IIB**. At the end two-pocket models are discussed: The possibility of a Suhl-Matthias-Walker coupling is discussed in section **IIC**, and is ruled out on the basis of disorder, and a McMillan coupling is discussed in section **IID**, which is ruled out based on spectroscopic and transport data.

I. THE SAMPLE AND EXPERIMENTAL METHODS

The devices reported in this work were fabricated in a similar method to those reported in ref^{S1}. First, NbSe₂ was exfoliated within a glovebox with an inert N₂ environment onto a silicon chip covered with 285nm of SiO₂. Next, WSe₂ was exfoliated on a PDMS stamp and examined to look for thin flakes. Once a suitable flake was found, it was aligned and brought into contact with a thin flake of NbSe₂. Next, the heterostructure was removed from the glovebox and tunnel contacts (5nm/80nm Ti/Au) were deposited on the WSe₂ barrier. Finally, ohmic contacts (5nm/80nm Ti/Au) were deposited directly on the NbSe₂ after Ar milling to remove oxide layers. The resulting device is shown in figure **S1**. The two junctions focused on in the main text are J7, on top of a 2ML NbSe₂ flake, with a tunneling resistance of $R_1 \approx 1.8\text{M}\Omega$, and J6, on top of a 4-8ML NbSe₂ region, with a resistance of $R_2 \approx 12\text{k}\Omega$.

As a part of the sample characterization the differential conductance of both junctions was measured at $T = 50\text{mK}$ (in a He³ – He⁴ dilution refrigerator) (shown in figure 3 of the main text). The extracted values for Δ are in line with the critical temperature T_c , estimated from the $G(V = 0)$ temperature dependence - see figure **S2**. This, as well as the data reported in^{S2}, shows that for few-layer samples, which are of main interest here, the order parameter Δ and the critical temperature T_c follow the BCS prediction $\Delta = 1.76k_bT_c$.

The high field measurements were performed at the "Laboratoire National des Champs Magnétiques Intenses" in Grenoble, France. The magnet used allowed for magnetic fields up to $H = 36\text{T}$.

The sample was cooled down to $T = 1.25\text{K}$ in a pumped He⁴ cryostat, and the differential conductance was measured using a standard lock-in technique with an excitation of $V_{lock-in} = 100\mu\text{V}$. Although the excitation voltage is relatively large, it does not lead to a significant smearing of the obtained spectrum as $eV_{lock-in} \ll 3.5k_B T \approx 360\mu\text{eV}$ (where $3.5k_bT$ is the FWHM of the Fermi distribution transition). Likewise the electrical noise, generated by the magnet flux noise is also smaller than the temperature - see figure **S3**. The sample was mounted on a rotating stage, the axis of which was perpendicular to the magnetic field. A field of $H = 2\text{T}$ was applied and the sample was rotated, while measuring the height of the coherence peaks. By maximizing the peak height the magnetic field was aligned with the plane of the sample, with a maximum deviation of up to 1° . A misalignment of $\sim 1^\circ$ (the maximum realistically possible in our experiment), gives a perpendicular component of the magnetic field smaller than 0.3 T, several times

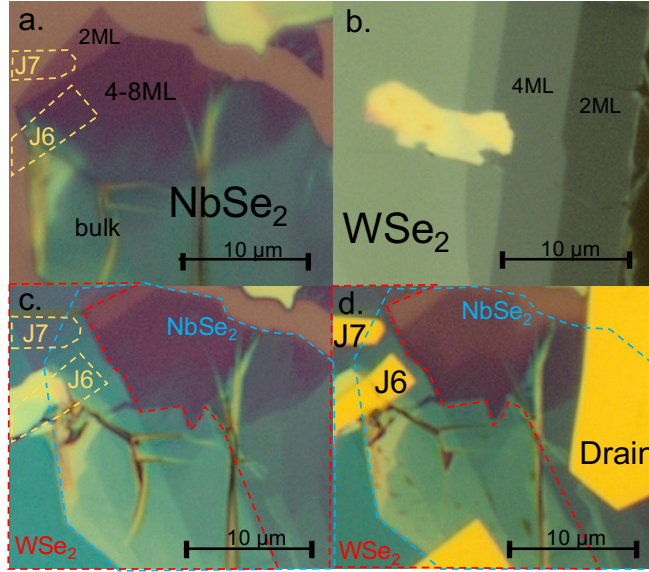


Figure S1 a. NbSe₂ exfoliated on SiO₂ from a PDMS stamp. Flake thickness is determined from the optical contrast. b. WSe₂ exfoliated on a PDMS stamp. Flake thickness is determined from the optical contrast. c. NbSe₂ – WSe₂ heterostructure formed by the deterministic transfer of the WSe₂. d. The final device with multiple tunnel junctions (J6, J7) and ohmic contacts (Drain).

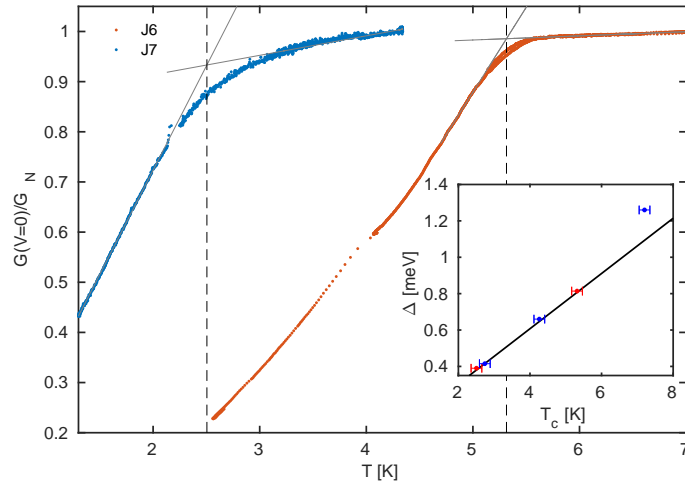


Figure S2 The temperature dependence of the zero voltage conductance, $G(V = 0)$, for devices J7 (2ML) and J6 (6ML). Inset the Δ vs the estimated T_c : for J7 and J6 (red dots), the data from^{S3} (blue circles) and the BCS result $\Delta = 1.76k_bT_c$ (black line).

smaller than the perpendicular critical field^{S4,S5}, thus it should not substantially decrease the observed critical field H_c .

A. $G(V)$ curve fitting

With the main goal of determining the order parameter as a function of the magnetic field, $\Delta(H)$, the following heuristic approach was adopted. Without a proper microscopic theory to describe the soft gapped spectrum in presence of weak inter-valley scattering, and with limited ability to discern the details of the density of states (DOS) at $T = 1.3K$, the simplest approach to take is to try several different models for the $G(V)$ traces and compare the results. Even though there are countless models that one can utilize the discussion here is limited to the following

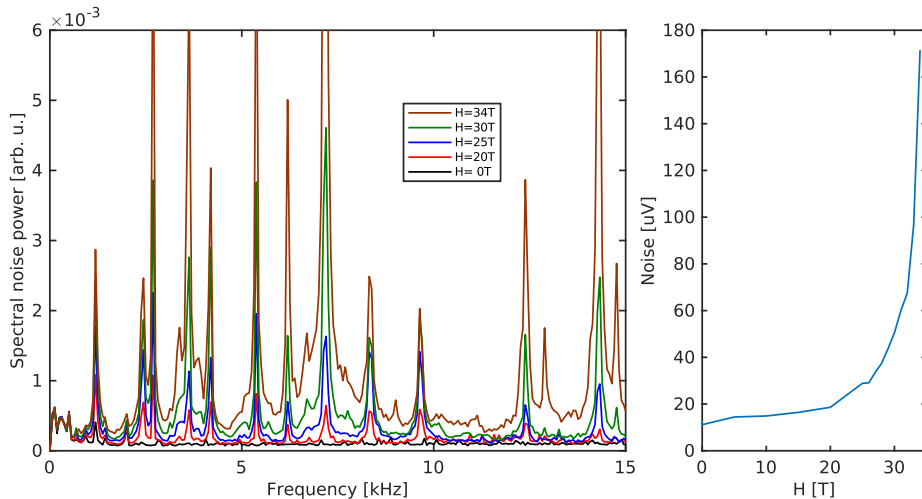


Figure S3 Electrical noise measured at $T = 1.2\text{K}$, across a $R = 10\text{k}\Omega$ resistor in a bandwidth of DC – 32kHz, as a function of the magnetic field. The left panel show the noise spectrum, while the right one shows the integrated noise voltage.

three: an effective temperature T^* with a BCS DOS, an Abrikosov-Gor'kov DOS (A-G DOS) ^{S6} and a Dynes DOS ^{S7}. At finite temperatures the $G(V)$ curve is obtained by convolving the DOS with a distribution $\approx 3.5k_B T$ wide (FWHM): $G(V) = \frac{1}{eR} \int_{-\infty}^{\infty} dE N(E) \frac{\partial f(E-V)}{\partial V}$, where $N(E)$ is the normalized density of states. If $3.5k_B T \approx \Delta$ this leads to a finite conductance at zero voltage bias. The Abrikosov-Gor'kov depairing model lowers the spectral gap below the order parameter Δ . When the depairing energy equals the order parameter, $\alpha(H) = \Delta(H)$ this leads to a gapless state, but even when $\alpha(H) < \Delta(H)$ along with a finite temperature the resulting $G(V)$ trace can be gapless. Lastly, the Dynes DOS is non-zero at $E = 0$, directly leading to a soft gap. To illustrate this a simple example is shown in figure S4 - the top panel show the BCS, Abrikosov-Gor'kov and Dynes densities of states, as well as the distribution function $\frac{\partial f(E-V)}{\partial V}$ for some parameter values, while the bottom panel shows the corresponding differential conductance traces. Although the BCS and the Abrikosov-Gor'kov DOS' are fully gapped the resulting spectra are quite similar, and resemble a gapples spectrum.

The parameters for the effective temperature model were the (field dependent) order parameter $\Delta(H)$ and the temperature $T^*(H)$. For the Abrikosov-Gor'kov and Dynes fits the temperature was fixed to $T = 1.25\text{K}$, while the depairing and Dynes energies were fitting parameters. The $\Delta(H)$ dependence obtained in this way, for both junctions and all three models, is shown on figure S5.

It is important to note that the values of these extra field dependent parameters, have no physical significance: the gap value is not self-consistently determined, nor should they be interpreted in the context of their usual meaning. They are rather just phenomenological parameters used to describe the obtained $G(V)$ spectra. To illustrate this figure S6 shows the self-consistent and experimentally obtained Δ versus the Abrikosov-Gor'kov and Dynes Γ parameters.

As this approach estimates Δ not based on the details of the $G(V)$ spectrum, but rather the energy scale of the (spectroscopic) gap, it is important to show that this is a robust feature. To this end figure S7 shows the $G(V)$ data from J7 at $H = 20\text{T}$, as well as several theoretical traces. The first of which is the Abrikosov-Gor'kov fit, followed by two traces with the same gap, but different depairing values, which demonstrate that the energy scale of the gap is dominantly set by Δ while the depth of the gap at $V = 0$ is set by the depairing. The last trace shows that the gap is significantly different than the one found at $H = 0$, contrary to what one might naively infer based on the colorplots shown in figure 3 of the main text.

Additionally the error of the Δ estimation can be performed in the following way: the log-likelihood distribution for the fitting parameters (given the data) is given by

$$\tilde{p}(\Delta, \tilde{x}) = - \frac{\langle (G_i - f(V_i, \Delta, \tilde{x}))^2 \rangle_i}{2\sigma^2}$$

where \tilde{x} stands for the additional model-dependent parameters and $\langle \dots \rangle_i$ denotes the average over all of the acquired points. σ , the noise of the measurement, can be estimated either directly from data, or by the root-mean-square error (RMSE) of the fit, both of which give similar results. The log-likelihood is not necessarily quadratic in Δ , as the fitting problem is nonlinear, but close to the maximum-likelihood point it can be approximately quadratic. Therefore

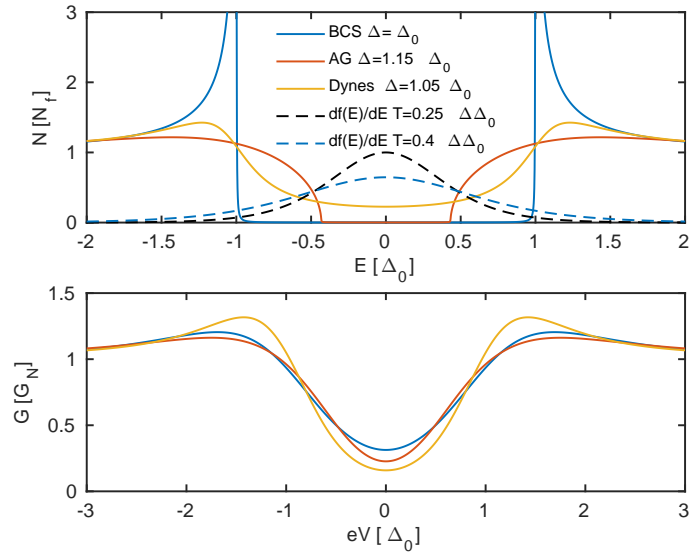


Figure S4 Top: The BCS density of states (blue, $\Delta = 1$), the Abrikosov-Gor’kov one (red, $\Delta = 1.15$, $\alpha = 0.38$) and the Dynes one (yellow, $\Delta = 1.05$, $\Gamma = 0.24$). The dashed lines are the derivatives of the Fermi distribution function for $T = 0.25\Delta$ (black) and $T = 0.4\Delta$ (blue). Bottom: the corresponding $G(V)$ traces. The BCS DOS was convolved with the higher temperature distribution function, while the other two were convolved with the lower temperature one.

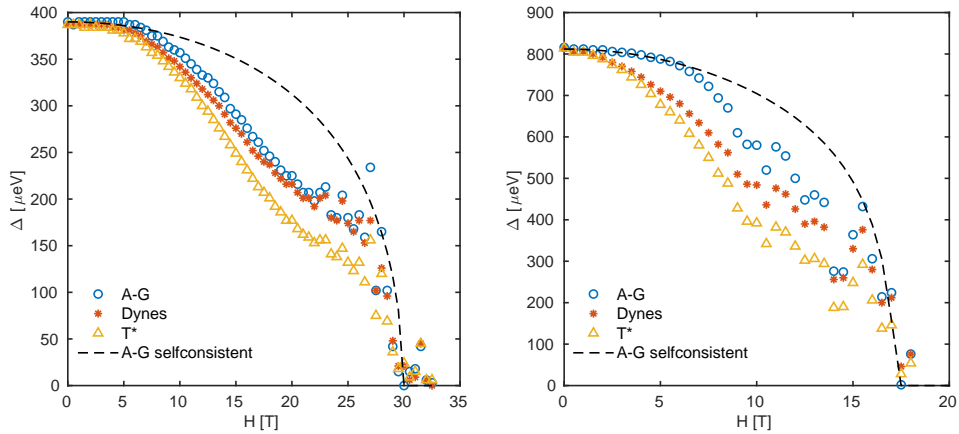


Figure S5 The extracted order parameters as function of the applied magnetic field using the three different $G(V)$ models, for the J7 (2ML, left panel), and J6 (4-8ML, right panel).

by fitting \tilde{p} near it’s maximal point with $-\frac{(\Delta-\tilde{\Delta})^2}{2\delta^2} + c$, where c is related to the RMSE and $\tilde{\Delta}$ is the best fit value, we obtain an estimate of the fit uncertainty δ_Δ . The Abrikosov-Gor’kov $\Delta(H)$ curve with errors estimated in this way is shown in figure 4 of the main text. We find that the uncertainty of the extracted values of Δ is roughly equal to the spread of the data, regardless of the $G(V)$ model. The experimental $G(V)$ traces and the Abrikosov-Gor’kov fits are shown on figure 3 of the main text. The fits obtained using the other two models are almost indistinguishable from the Abrikosov-Gor’kov one.

B. DOS broadening

Here we address the issue of in-gap states and the broadening of the coherence peaks. Indeed, the broadening parameters obtained from the fits are larger than expected from self-consistent Abrikosov-Gor’kov theory^{S8} or a self-consistent Dynes model^{S9} (see figure S6). Moreover, at the critical field the broadening parameter is larger than theoretically allowed $2\alpha_c = \Delta(H = 0)$.

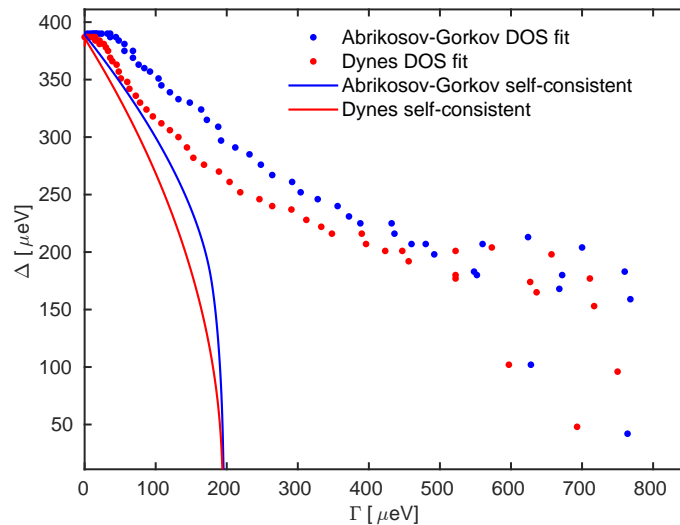


Figure S6 The order parameter Δ as a function of the Abrikosov-Gor'kov depairing (blue) and the Dynes energy (red) for J7, obtained from the fitting (dots) and the self-consistent gap equation (full lines).

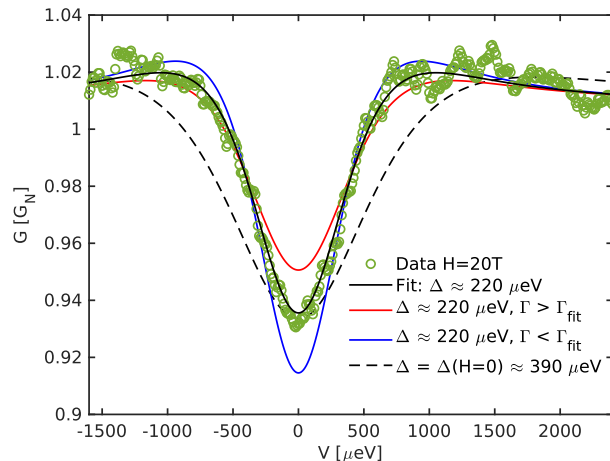


Figure S7 The experimental data from J7 at $H = 20\text{T}$ (green circles), the Abrikosov-Gor'kov fit (solid black) and two traces with the same Δ but different depairings and a trace with $\Delta = \Delta(H = 0)$ with a depairing which fits the "depth" of the spectroscopic gap.

There are several possible reasons for this unexpected DOS broadening:

1. At the K/K' points, the two spins have slightly different dispersions and densities of states — this can lead to broadening of the peak^{S10}. While Ref.^{S10} assumes superconductivity arising from Coulomb interactions, the same broadening phenomenon will appear for all pairing mechanisms. This is likely the reason why in both our work and that of^{S2}, reproduced here in figure S8, the effective temperature is much higher than the measurement temperature. This is the case even at (higher) temperatures where there should be good electron-phonon coupling, and where the electron temperature should thus be that of the refrigerator (~ 100 mK and above). Besides this, the following could also contribute to the broadening of the DOS.
2. In-gap states may appear in triplet superconductors because of field-induced gap nodes at the Fermi surface^{S11}. Such nodes would occur along the Γ -M directions when E_Z (the Zeeman energy) exceeds the order parameter Δ_s . This means that only the Γ pockets would be affected and not the K/K' ones. Since electrons tunnel into the K/K' pockets (see Section IIC1), some K/K'- Γ coupling would have to be present for such nodes to affect our measured density of states.
3. Inelastic tunneling; energy loss due to defects in the barrier will broaden the $G(V)$ characteristic^{S12,S13}.

4. Coupling of the charge density waves via phonons either to the quasiparticles, or to amplitude fluctuations (Higgs mode) of the order parameters^{S14}.

These various factors are difficult to disentangle; however, none of them significantly affects the energy gap, which can be determined with high precision from the fits, as was shown in this section.

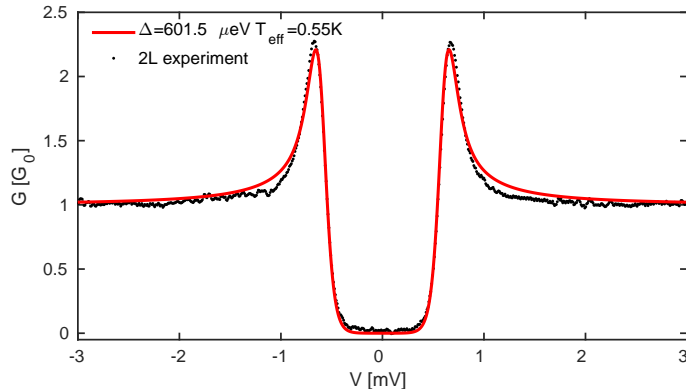


Figure S8 The bi-layer tunneling spectrum from^{S2} (reproduced with the authors' permission), along with a BCS fit.

C. Estimate of Inter-valley (K/K') and Total Scattering Times

Intervalley Scattering Time: Ref.^{S15} gives $H_{||}^c$ as a function of temperature for different τ_{iv} , the scattering time between K and K' points, for an Ising superconductor. While the theory in Ref.^{S15} does not include a triplet order parameter or two-pocket coupling, this should not change the order of magnitude of estimates of $H_{||}^c$ for a given τ_{iv} and vice versa. (This can be seen in Figure 1c of the main text.) In our case $E_{SO}/(k_B T_c) \sim 20$. From Figure 5c in Ref.^{S15}, and using our experimental values for T , T_c and $H_{||}^c$ we estimate $h/\tau_{iv} \approx k_B T_{cs}$. h/τ_{iv} is therefore on the order of $\Delta_s \approx 400 \mu\text{eV}$.

Total Scattering Time: In Ref.^{S16}, the mean free path ℓ for a bilayer NbSe₂ device was estimated to be 17 nm from Hall measurements. Thus, the total scattering time, including all intra- and inter-valley processes, is $\tau = \ell/v_F$. As $v_F \approx 5 \cdot 10^4$ m/s^{S3}, this gives $\tau \approx 340$ fs. Now, our bilayer device is more disordered than that of Ref.^{S16}: whereas $H_c^{||}$ in Ref.^{S16} is the same as in our case, their critical temperature is 5K, as opposed to 2.6K for us. Thus, $1/\tau \approx 10$ meV can be considered a lower limit for the total scattering time $1/\tau$ in our bilayer device. This is consistent with the estimate above of the inter-valley scattering rate, that is to say $1/\tau > 1/\tau_{iv}$.

From the above two estimates, and from the fact that single-particle $\Gamma - K/K'$ scattering (McMillan coupling) does not seem to be important for our devices (cf. Section IID below), we conclude that intra-pocket (K-K, K'-K' or $\Gamma - \Gamma$) is the dominant disorder-induced scattering.

II. THEORY

In this appendix, we calculate the superconducting energy gap of a monolayer superconductor without an inversion center and in the presence of an in-plane magnetic field. In Sec. II.A, we introduce the appropriate Hamiltonian. In Sec. II. B, we study the density of states in the presence of singlet and triplet pairing in a simplified model restricted to the K/K' pockets. In Secs. II.C & II.D, we address the interplay between the K/K' and Γ pockets within two different models taking into account singlet pairing only : in Sec. II.C, we use the so-called Suhl-Matthias-Walker coupling describing inter-pocket pairing or Cooper pair tunneling, whereas in Sec. II.D, we use the so-called MacMillan coupling describing inter-pocket single-particle tunneling or scattering.

A. The model Hamiltonian

The model Hamiltonian is a sum of the free part H_0 which defines our band structure model, the disorder Hamiltonian H_{dis} and the interaction H_{int} ,

$$H = H_0 + H_{dis} + H_{int}. \quad (S1)$$

Our band structure model includes the Nb derived bands. The crossing of the Nb derived band with the Fermi level gives rise to a hole-like pocket centered at Γ as well as a pair of hole-like pockets centered at $K(K')$ labeled by the valley index, $\eta = \pm 1$. In result, we have

$$H_0 = \sum_{\eta} \sum_{\mathbf{k}, s} \xi_{\mathbf{k}}^K a_{\eta\mathbf{k}s}^{\dagger} a_{\eta\mathbf{k}s} + \sum_{\eta} \sum_{\mathbf{k}, s, s'} (\gamma_{\eta}^K - \mathbf{B}) \cdot \boldsymbol{\sigma}_{ss'} a_{\eta\mathbf{k}s}^{\dagger} a_{\eta\mathbf{k}s'} + \sum_{\mathbf{k}, s} \xi_{\mathbf{k}}^{\Gamma} b_{\mathbf{k}s}^{\dagger} b_{\mathbf{k}s} + \sum_{\mathbf{k}, s, s'} (\gamma_{\mathbf{k}}^{\Gamma} - \mathbf{B}) \cdot \boldsymbol{\sigma}_{ss'} b_{\mathbf{k}s}^{\dagger} b_{\mathbf{k}s'}. \quad (S2)$$

Here $a_{\eta\mathbf{k}s}^{\dagger}$ and $b_{\mathbf{k}s}^{\dagger}$ are the creation operators in the K/K' and Γ pockets, respectively, $\xi_{\mathbf{k}}^{\Gamma(K)}$ is the spin-independent part of the band energy measured relative to Fermi energy, $\boldsymbol{\sigma} = (\sigma_x, \sigma_y, \sigma_z)$ is the vector of Pauli matrices, $\gamma_{\eta}^K = -\gamma_{\eta}^K$ and $\gamma_{\mathbf{k}}^{\Gamma} = -\gamma_{\mathbf{k}}^{\Gamma}$ are the anti-symmetric SOC terms arising from the lack of inversion symmetry and $\mathbf{B} = E_Z \hat{x}$ is the Zeeman field, i.e. the magnetic field which absorbs the prefactor $g\mu_B/2$ that includes the g -factor and Bohr magneton. We use the notation $\bar{\eta} = -\eta$, $\bar{\mathbf{k}} = -\mathbf{k}$. For the K -pocket and Γ -pocket we consider the Ising SOC of the form,

$$\gamma_{\eta}^K = \eta E_{SO}^K \hat{z}, \quad \gamma_{\mathbf{k}}^{\Gamma} = E_{SO}^{\Gamma} \cos(3\varphi_{\hat{\mathbf{k}}}) \hat{z}, \quad (S3)$$

where $\varphi_{\hat{\mathbf{k}}}$ is the angle formed by the momentum unit vector $\hat{\mathbf{k}}$ of an electron with the k_x direction. Within the Γ pocket, the SOC $\gamma_{\mathbf{k}}^{\Gamma}$, Eq. (S3), changes sign six times at the ΓM lines. In the K and K' pockets, it is constant and antiparallel.

The presence of randomly distributed scalar impurities gives rise to a scattering potential,

$$H_{dis}(\mathbf{r}) = \sum_l U_0(\mathbf{r} - \mathbf{R}_l), \quad (S4)$$

where \mathbf{R}_l is the location of the l th impurity scattering center. Singlet pairing as well as inter-valley triplet pairing in K/K' pockets is not sensitive to intra-valley scattering. To study the effect of inter-valley scattering, we consider a short-range impurity potential such that $U_0(\mathbf{k} - \mathbf{k}') = U_0$. The effect of the impurity potential is described within the self-consistent Born approximation by the appropriate self-energy $\hat{\Sigma}$, which we do not write here explicitly. $\hat{\Sigma}$ is proportional to the scattering rate $1/\tau_{iv} = \pi n_{imp} N_0 U_0^2$, where n_{imp} is the impurity density and N_0 is the normal state density of states per spin species. Superconductivity within the Γ pocket is sensitive to intra-pocket scattering at finite magnetic fields. We characterize it by a scattering rate $1/\tau_{\Gamma}$. As it involves a small momentum transfer, both short-and long-range impurities contribute. Thus we expect $1/\tau_{\Gamma} \gg 1/\tau_{iv}$. In the following, we set $k_B = 1$.

The interaction Hamiltonian, H_{int} in Eq. (S1), contains the superconducting pairing interactions

$$H_{int} = \frac{1}{2} \sum_{\eta, \eta'} \sum_{s_i, s'_i, \mathbf{k}, \mathbf{k}'} V_{s_1 s_2, s'_1 s'_2}^{KKK}(\mathbf{k}, \eta; \mathbf{k}', \eta') a_{\eta\mathbf{k}s_1}^{\dagger} a_{\bar{\eta}\bar{\mathbf{k}}s_2}^{\dagger} a_{\bar{\eta}'\bar{\mathbf{k}}'s'_2} a_{\eta'\mathbf{k}'s'_1} + \frac{1}{2} \sum_{s_i, s'_i, \mathbf{k}, \mathbf{k}'} V_{s_1 s_2, s'_1 s'_2}^{\Gamma\Gamma}(\mathbf{k}, \mathbf{k}') b_{\mathbf{k}s_1}^{\dagger} b_{\mathbf{k}s_2}^{\dagger} b_{\bar{\mathbf{k}}'s'_2} b_{\mathbf{k}'s'_1} \quad (S5)$$

$$+ \frac{1}{2} \sum_{\eta} \sum_{s_i, s'_i, \mathbf{k}, \mathbf{k}'} V_{s_1 s_2, s'_1 s'_2}^{K\Gamma}(\mathbf{k}, \eta; \mathbf{k}') a_{\eta\mathbf{k}s_1}^{\dagger} a_{\bar{\eta}\bar{\mathbf{k}}s_2}^{\dagger} b_{\bar{\mathbf{k}}'s'_2} b_{\mathbf{k}'s'_1} + \frac{1}{2} \sum_{\eta'} \sum_{s_i, s'_i, \mathbf{k}, \mathbf{k}'} V_{s_1 s_2, s'_1 s'_2}^{\Gamma K}(\mathbf{k}; \mathbf{k}', \eta') b_{\mathbf{k}s_1}^{\dagger} b_{\mathbf{k}s_2}^{\dagger} a_{\bar{\eta}'\bar{\mathbf{k}}'s'_2} a_{\eta'\mathbf{k}'s'_1}.$$

where V^{KK} and $V^{\Gamma\Gamma}$ are the intra-pocket pairing interactions in the $K(K')$ and Γ pockets, respectively, whereas $V^{K\Gamma}$ and $V^{\Gamma K}$ are the inter-pocket pairing interactions.

We introduce the two order parameters (OPs) in the standard way,

$$\underline{\Delta}_{s_1 s_2}^{K, \eta}(\mathbf{k}) = \frac{1}{V} \sum_{\mathbf{k}', s'_1, s'_2} \left[\sum_{\eta'} V_{s_1 s_2, s'_1 s'_2}^{KKK}(\mathbf{k}, \eta; \mathbf{k}', \eta') \langle a_{\bar{\eta}'\bar{\mathbf{k}}'s'_2} a_{\eta'\mathbf{k}'s'_1} \rangle + V_{s_1 s_2, s'_1 s'_2}^{K\Gamma}(\mathbf{k}, \eta; \mathbf{k}') \langle b_{\bar{\mathbf{k}}'s'_2} b_{\mathbf{k}'s'_1} \rangle \right],$$

$$\underline{\Delta}_{s_1 s_2}^{\Gamma}(\mathbf{k}) = \frac{1}{V} \sum_{\mathbf{k}', s'_1, s'_2} \left[V_{s_1 s_2, s'_1 s'_2}^{\Gamma\Gamma}(\mathbf{k}; \mathbf{k}') \langle b_{\bar{\mathbf{k}}'s'_2} b_{\mathbf{k}'s'_1} \rangle + \sum_{\eta'} V_{s_1 s_2, s'_1 s'_2}^{\Gamma K}(\mathbf{k}; \mathbf{k}', \eta') \langle a_{\bar{\eta}'\bar{\mathbf{k}}'s'_2} a_{\eta'\mathbf{k}'s'_1} \rangle \right], \quad (S6)$$

where V is the volume of the system, and $\langle \dots \rangle$ stands for the thermodynamic and quantum mechanical averaging. They can be represented in the standard matrix form,

$$\underline{\Delta}^{\Gamma(K,\eta)}(\mathbf{k}) = \left[\psi^{\Gamma(K,\eta)}(\mathbf{k}) + \mathbf{d}^{\Gamma(K,\eta)}(\mathbf{k}) \cdot \boldsymbol{\sigma} \right] i\sigma_2. \quad (\text{S7})$$

Here $\psi^{\Gamma(K,\eta)}(\mathbf{k})$ and $\mathbf{d}^{\Gamma(K,\eta)}(\mathbf{k})$ parametrize the singlet and triplet components of the OP, respectively. For simplicity, we assume the singlet OPs to be isotropic, $\psi^{\Gamma(K,\eta)}(\mathbf{k}) = \Delta_s^{\Gamma(K)}$.

Interactions in Eq. (S5) may have components in both singlet and triplet channels,

$$V^{\beta\beta'} = V_s^{\beta\beta'} + V_t^{\beta\beta'} \quad (\text{S8})$$

where β, β' refer to the pocket index. For the singlet pairing we take

$$V_s^{\beta\beta'} = v^{\beta\beta'} [i\sigma_y]_{s_1 s_2} [i\sigma_y]_{s'_1 s'_2}^*. \quad (\text{S9})$$

The hermiticity condition yields $[v^{\Gamma\Gamma}]^* = v^{\Gamma\Gamma}$, $[v^{KK}]^* = v^{KK}$, and $[v^{\Gamma K}]^* = v^{K\Gamma}$. Furthermore, we take inter-pocket couplings real which makes them equal, $v^{\Gamma K} = v^{K\Gamma}$, and consider attractive interactions, $v^{\beta\beta'} < 0$ for definiteness.

In this SI, the triplet OP will be considered in the K/K' pockets only, $\mathbf{d}^K = \mathbf{d}_\eta$,

$$\mathbf{d}_\eta = \hat{\gamma}_\eta (\eta_{E1}\hat{x} + \eta_{E2}\hat{y} + \eta_A\hat{z}) \quad (\text{S10})$$

where η_A and $\eta_{E1(2)}$ are triplet OPs transforming trivially and non-trivially under D_{3h} . Eq. (S10) leads us to the effective interaction,

$$V_t^{KK}(\eta, \eta') = \sum_{j=1,2} v_t [\hat{\gamma}_\eta \sigma_j i\sigma_2]_{s_1 s_2} [\hat{\gamma}_{\eta'} \sigma_j i\sigma_2]_{s'_1 s'_2}^* + v_{tz} [\hat{\gamma}_\eta \sigma_3 i\sigma_2]_{s_1 s_2} [\hat{\gamma}_{\eta'} \sigma_3 i\sigma_2]_{s'_1 s'_2}^*. \quad (\text{S11})$$

As shown in Ref.^{S17}, the magnetic field couples the singlet order parameter Δ_s and the equal spin triplet order parameter η_{E2} . For the purpose of fitting the data, we assume that singlet pairing is dominant and that the temperature is larger than the critical temperature of all the possible triplet pairings. In that case, we can set $\eta_A = \eta_{E1} = 0$ and keep only the singlet and the η_{E2} -triplet order parameters.

We define the transition temperature T_{cs} (T_{ct}) by setting $E_Z = E_{\text{SO}} = \Gamma = 0$ and keeping only the Δ_s (η_{E2}) OP in Eq. (S7). The relation between T_{cs} and v_s is $T_{cs} = 2\Lambda e^{\gamma_E} \pi^{-1} \exp[-1/2N|v_s|]$, where Λ is a cutoff for the high energy attraction, N is the density of states per spin summed over all superconducting pockets, and γ_E is Euler's constant. Similarly, for T_{ct} , we have $T_{ct} = 2\Lambda e^{\gamma_E} \pi^{-1} \exp[-1/2N|v_t|]$. For the analysis, we use the transition temperatures rather than the interaction amplitudes as parameters.

The Bogoliubov-de Gennes (BdG) Hamiltonian for electrons in the K/K' and Γ pockets reads

$$\hat{H}_{\text{BdG}}^{\Gamma(K,\eta)} = \begin{bmatrix} \xi_{\mathbf{k}} + \left[\gamma_{\mathbf{k}(\eta)}^{\Gamma(K)} - \mathbf{B} \right] \cdot \boldsymbol{\sigma} & \underline{\Delta}^{K(\Gamma)} \\ \underline{\Delta}^{\Gamma(K)\dagger} & -\xi_{\mathbf{k}} + \left[\gamma_{\mathbf{k}(\eta)}^{\Gamma(K)} + \mathbf{B} \right] \cdot \boldsymbol{\sigma}^T \end{bmatrix}. \quad (\text{S12})$$

Now, we will consider different scenarios: In subsection IIB, we will consider both singlet and triplet pairing in a simplified model neglecting the Γ pocket. In subsections IIC and IID, we consider the effect of the Γ pocket, but neglecting triplet pairing.

B. Simplified model without the Γ pocket

Focusing on the K pocket with triplet component of the OP, the dispersion relation is determined by the solution of the equation

$$\det \left[E\hat{\sigma}_0 - \hat{H}_{\text{BdG}}^{K,\eta} \right] = 0 \quad (\text{S13})$$

for E , where $\hat{\sigma}_0$ is the 4×4 unit matrix. We choose the phase of the singlet OP Δ_s to be 0. The coupling between the singlet and triplet order parameters imposes their relative phases such that $\mathbf{d}_\eta = i \text{sign}(E_Z) \hat{\gamma}_\eta \Delta_{tB} \hat{y}$ with Δ_{tB} real and positive. The physically relevant solution for the energy is

$$E(\xi_{\mathbf{k}}) = \left(\xi_{\mathbf{k}}^2 + E_{\text{SO}}^2 + E_Z^2 + \Delta_s^2 + \Delta_{tB}^2 \right. \\ \left. - 2\sqrt{\xi_{\mathbf{k}}^2 (E_{\text{SO}}^2 + E_Z^2) + (|E_Z|\Delta_s - E_{\text{SO}}\Delta_{tB})^2} \right)^{1/2}. \quad (\text{S14})$$

The dispersion $E(\xi_{\mathbf{k}})$ has a minimum at $\xi_{\mathbf{k}} = \sqrt{\rho^2 - P^2/\rho^2}$, where we introduced the notation $\rho = \sqrt{E_{\text{SO}}^2 + E_Z^2}$ and $P = |E_Z|\Delta_s - E_{\text{SO}}\Delta_{tB}$, which gives the superconducting energy gap

$$\Delta = \frac{1}{\rho} (E_{\text{SO}}\Delta_s + |E_Z|\Delta_{tB}). \quad (\text{S15})$$

1. Without inter-valley scattering: Quasiclassical Green functions

The coupled order parameters and density of states can be computed using quasiclassical Green functions. In the absence of inter-valley scattering, we obtain^{S18}

$$\nu(E) = 2N_0\Re \left[\frac{\omega_n \text{sign}(\Sigma)}{\sqrt{2} [\Sigma - 2\rho^2 + \text{sign}(\Sigma)\sqrt{\Sigma^2 - 4P^2}]^{1/2}} \left(1 + \frac{|\Sigma|}{\sqrt{\Sigma^2 - 4P^2}} \right) \right]_{i\omega_n \rightarrow E+i\delta}, \quad (\text{S16})$$

$$\Delta_s = 2\pi T |v_s| \sum_{\omega_n > 0} \frac{1}{\sqrt{2} [\Sigma - 2\rho^2 + \sqrt{\Sigma^2 - 4P^2}]^{1/2}} \left[\Delta_s \left(1 + \frac{\Sigma - 2E_Z^2}{\sqrt{\Sigma^2 - 4P^2}} \right) + \Delta_{tB} \frac{2|E_Z|E_{\text{SO}}}{\sqrt{\Sigma^2 - 4P^2}} \right], \quad (\text{S17})$$

$$\Delta_{tB} = 2\pi T |v_t| \sum_{\omega_n > 0} \frac{1}{\sqrt{2} [\Sigma - 2\rho^2 + \sqrt{\Sigma^2 - 4P^2}]^{1/2}} \left[\Delta_{tB} \left(1 + \frac{\Sigma - 2E_{\text{SO}}^2}{\sqrt{\Sigma^2 - 4P^2}} \right) + \Delta_s \frac{2|E_Z|E_{\text{SO}}}{\sqrt{\Sigma^2 - 4P^2}} \right], \quad (\text{S18})$$

where $\omega_n = \pi T(2n+1)$ are fermionic Matsubara frequencies and we introduced the notation $\Sigma = \omega_n^2 + \rho^2 + \Delta_s^2 + \Delta_{tB}^2$. The density of states Eq. (S16) displays a superconducting energy gap Δ . Furthermore, there is a partial ‘‘mirage’’ gap^{S19} centered around $E = \pm\sqrt{\rho^2 + \Delta_s^2 + \Delta_{tB}^2}$.

In general, the coupled self-consistency equations can be solved numerically. The fit shown in the main text was obtained that way. However, simplifications are possible in the limit $E_{\text{SO}} \gg \Delta_0$, where Δ_0 is the zero-temperature, zero-field singlet order parameter. In that case, Eqs. (S17) and (S18) may be combined into one equation for the gap Δ ,

$$\frac{\left[2\pi T |v_s| \sum_{\omega_n > 0} \frac{1}{\sqrt{\omega_n^2 + \Delta^2}} - 1 \right] \left[2\pi T |v_t| \sum_{\omega_n > 0} \frac{1}{\sqrt{\omega_n^2 + \Delta^2}} - 1 \right]}{|v_t|E_{\text{SO}}^2 \left[2\pi T |v_s| \sum_{\omega_n > 0} \frac{1}{\sqrt{\omega_n^2 + \Delta^2}} - 1 \right] + |v_s|E_Z^2 \left[2\pi T |v_t| \sum_{\omega_n > 0} \frac{1}{\sqrt{\omega_n^2 + \Delta^2}} - 1 \right]} = 2\pi T \sum_{\omega_n > 0} \frac{1}{\sqrt{\omega_n^2 + \Delta^2}} \frac{1}{\omega_n^2 + \rho^2} \quad (\text{S19})$$

The density of states at $|E| \ll E_{\text{SO}}$ acquires a BCS form,

$$\nu(E) = \nu_0 \frac{|E|}{\sqrt{E^2 - \Delta^2}} \theta(|E| - \Delta). \quad (\text{S20})$$

2. With inter-valley scattering: Landau expansion

To study the effect of disorder on a qualitative level, we employ a Landau expansion valid close to the critical temperature. Considering the model Hamiltonian above and using quasiclassical methods the difference of the thermodynamic potential in superconducting and normal state Ω may be written in the form of a Landau expansion as

$$(V^2 N_0)^{-1} \Omega(\Delta_s, \Delta_{tB}) = \Omega^{(2)} + \Omega^{(4)}. \quad (\text{S21})$$

Here $\Omega^{(2)}$ contains the terms quadratic in the OPs, and $\Omega^{(4)}$ contains the quartic terms. For $\Omega^{(2)}$, we have

$$\Omega^{(2)} = A_1 \Delta_s^2 + A_2 \Delta_{tB}^2 + 2A_3 \Delta_s \Delta_{tB}. \quad (\text{S22})$$

Denoting $\tilde{\omega}_n = \omega_n + \text{sgn}(\omega_n)1/\tau_{iv}$, the coefficients are given as^{S20},

$$A_1 = 2\pi T \sum_{\omega_n > 0} \frac{\tilde{\omega}_n E_Z^2}{\omega_n [\tilde{\omega}_n (E_Z^2 + \omega_n^2) + \omega_n E_{\text{SO}}^2]} + \ln \frac{T}{T_{cs}}, \quad (\text{S23})$$

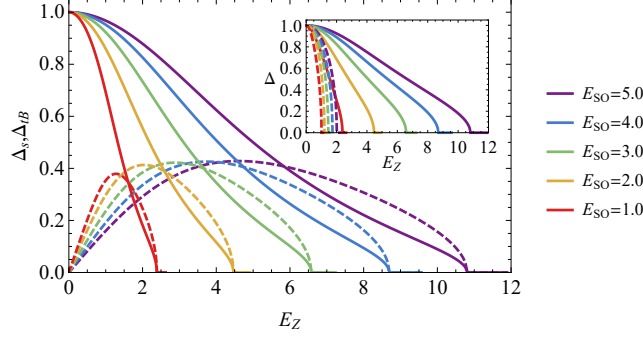


Figure S9 Effect of the magnitude of the spin-orbit coupling: The singlet Δ_s (solid lines) and triplet Δ_{tB} (dashed lines) OPs as a function of the field for different values of E_{SO} with parameters $T = 0.75T_{cs}$, $T_{ct} = 0.7T_{cs}$, $\tau_{iv}^{-1} = 0.001T_{cs}$. The inset shows the superconducting gap Δ for different values of E_{SO} and with the same parameters as the main graph, the solid lines are with the triplet component and the dashed lines are for a singlet-only superconductor ($T_{ct} = 0$). E_Z, E_{SO} are in units of T_{cs} . $\Delta, \Delta_s, \Delta_{tB}$ are normalized to the value of $\Delta = \Delta_s$ at $E_Z = 0$.

$$A_2 = 2\pi T \sum_{\omega_n > 0} \frac{\tau_{iv}^{-1} (E_Z^2 + \omega_n^2) + \omega_n E_{SO}^2}{\omega_n [\tilde{\omega}_n (E_Z^2 + \omega_n^2) + \omega_n E_{SO}^2]} + \ln \frac{T}{T_{ct}}, \quad (\text{S24})$$

$$A_3 = 2\pi T \sum_{\omega_n > 0} \frac{(-E_Z) E_{SO}}{\tilde{\omega}_n (E_Z^2 + \omega_n^2) + \omega_n E_{SO}^2}. \quad (\text{S25})$$

For succinctness, we do not provide here the full expression for $\Omega^{(4)}$ and only write the term corresponding to the singlet OP

$$\Omega_s^{(4)} = -\pi T_{cs} \sum_{\omega'_n > 0} D_1(\omega'_n) \Delta_s^4, \quad (\text{S26})$$

where

$$D_1(\omega) = \frac{1}{2 [\tilde{\omega} (E_Z^2 + \omega^2) + \omega E_{SO}^2]^4} \left[-\omega (\omega \tilde{\omega} + E_{SO}^2)^4 + 2E_Z^2 \omega (\tilde{\omega}^2 - E_{SO}^2) (\omega \tilde{\omega} + E_{SO}^2)^2 + E_Z^4 (3\omega \tilde{\omega}^4 + 2E_{SO}^2 \tilde{\omega}^2 (\tau_{iv}^{-1} + \tilde{\omega}) - \omega E_{SO}^4) \right]. \quad (\text{S27})$$

and where $\omega'_n = \pi T_{cs} (2n + 1)$. In the limit $E_{SO} = 0$ and no triplet OP, $\Delta_{tB} = 0$, derivation of the thermodynamic potential (S21) by the singlet OP reproduces the self consistency equation found in Ref. S21. Equipped with the thermodynamic potential, the OPs are found by the process of minimization.

Using the Landau expansion, we can obtain a qualitative understanding of the way the different parameters affect Δ_s , Δ_{tB} and Δ as a function of the field. We start with the case of negligible inter-valley scattering. In Fig. S9, we see that for large enough E_{SO} the effect of increasing E_{SO} is only to stretch the lines for larger critical fields E_{Zc} but otherwise keeping the shape of lines as they are. In Fig. S10, we see that the effect of increasing T_{ct} is to obtain larger critical fields E_{Zc} by increasing the triplet component in the superconducting phase, specifically we see that for larger T_{ct} we get a steeper rise of the triplet component at low fields.

We now turn to the effect of disorder. The impurity scattering potential has a broadening effect on the peak of the density of states but does not affect the form of the effective order parameter Δ appearing in the density of states significantly (though the superconducting energy gap may differ), hence we use (S15) as an estimation also in the presence of weak inter-valley scattering. In the presence of the in-plane magnetic field, the scattering off the scalar impurities causes a spin flip with finite probability, and makes the scalar impurity to behave effectively as a magnetic impurity with a field-dependent concentration. While the problem is captured by the Abrikosov-Gor'kov theory of magnetic impurities^{S22} in some parameter regimes, the general form of the self-consistency equation differs from the standard situation because the spin splitting E_{SO} intervenes as an additional energy scale.

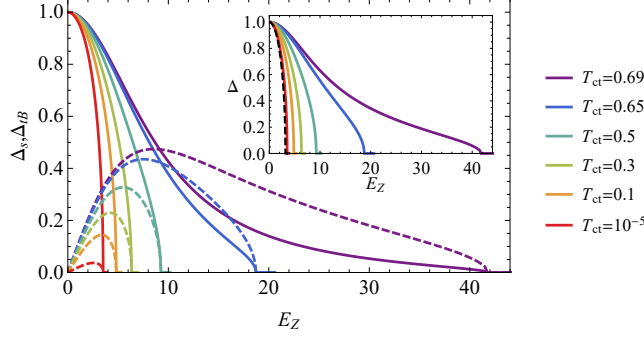


Figure S10 Effect of the triplet pairing: The singlet Δ_s (solid lines) and triplet Δ_{tB} (dashed lines) OPs as a function of the field for different values of T_{ct} with parameters $T = 0.7T_{cs}$, $E_{SO} = 8.0T_{cs}$, $\tau_{iv}^{-1} = 0$. The inset shows the superconducting gap Δ for different values of T_{ct} and with the same parameters as the main graph. The black dashed line is the superconducting gap for a singlet-only superconductor ($T_{ct} = 0$). E_Z, T_{ct} are in units of T_{cs} . $\Delta, \Delta_s, \Delta_{tB}$ are normalized to the value of $\Delta = \Delta_s$ at $E_Z = 0$.

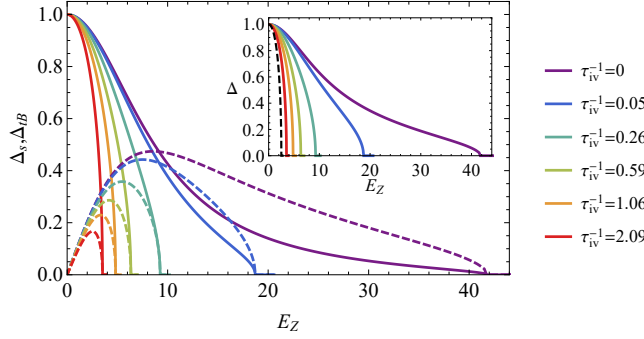


Figure S11 Effect of disorder: The singlet Δ_s (solid lines) and triplet Δ_{tB} (dashed lines) OPs as a function of the field for different values of τ_{iv}^{-1} with parameters $T = 0.7T_{cs}$, $E_{SO} = 8.0T_{cs}$, $T_{ct} = 0.69T_{cs}$. The inset shows the superconducting gap Δ for different values of τ_{iv}^{-1} and with the same parameters as the main graph. The red dashed line is the superconducting gap for a singlet-only superconductor ($T_{ct} = 0$), and with $\tau_{iv}^{-1} = 2.09T_{cs}$. E_Z, τ_{iv}^{-1} are in units of T_{cs} . $\Delta, \Delta_s, \Delta_{tB}$ are normalized to the value of $\Delta = \Delta_s$ at $E_Z = 0$.

The parameters corresponding to the lines with the highest critical fields in Figs. S10 and S11 are identical. The τ_{iv}^{-1} parameters in Fig. S11 were chosen so that identical colors in Figs. S10 and S11 will have approximately the same critical field. In Fig. S11 we see that by increasing τ_{iv}^{-1} we negate the affect of having $T_{ct} > 0$. Comparison of the OPs suppression obtained in Fig. S10 by decreasing T_{ct} to the suppression obtained in Fig. S11 by increasing τ_{iv}^{-1} shows that in the latter process we can retain a relatively steep increase of the triplet OP even for small critical fields, while in Fig. S10 the decrease in the critical field is accompanied by a faster decrease in slope of the triplet. The reason for this is that, even though increasing τ_{iv}^{-1} in Fig. S11 suppresses superconductivity, we still keep a high T_{ct} , which strengthens the triplet component, while in Fig. S10 the suppression of superconductivity is achieved by direct suppression of the triplet order parameter. The gap contains contributions of both the triplet and singlet order parameters. As the triplet order parameter is affected more strongly by a suppression of T_{ct} than by increase in τ_{iv}^{-1} the same is true for the gap. Compared to the triplet order parameter taken separately, the distinction between $\Delta(H)$ in the two cases is less pronounced as long as the singlet order parameter makes a dominant contribution to the gap.

C. Two-pocket superconductivity in NbSe₂ - Suhl-Matthias-Walker coupling

In few-layer NbSe₂ the Se derived Fermi pockets, observed in the bulk^{S23}, disappear^{S24}, and only the Nb derived pockets close to the K/K' and Γ points are left. Here we discuss the multi-pocket effects assuming a Suhl-Matthias-Walker^{S25} type coupling between pockets. This coupling describes the the inter-pocket Cooper pair tunneling process.

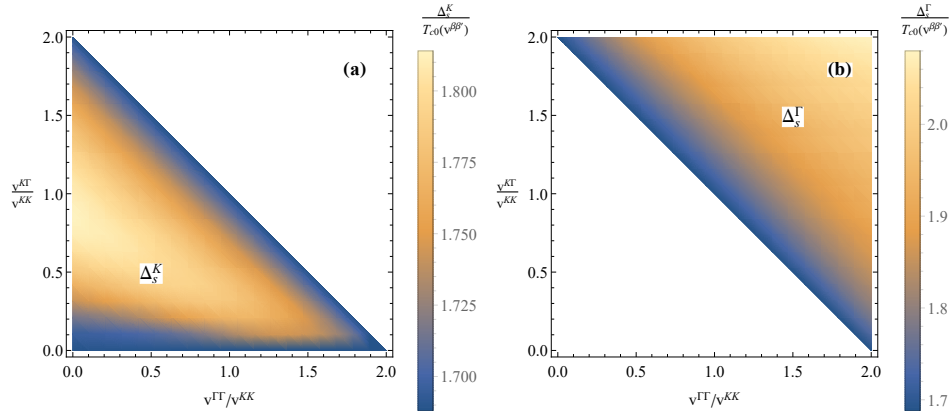


Figure S12 The OPs at $E_Z = 0$ for different values of $v^{\Gamma\Gamma}/v^{KK}$ and $v^{K\Gamma}/v^{KK}$, as calculated by numerically solving the two self-consistency equations. The plots show the larger OP, which is Δ_s^K in the region of panel (a) and Δ_s^Γ in the region of panel (b). We take $N_0 v^{KK} = -0.5$, and $T/T_{c0} = 0.5$ where T_{c0} is given by Eq. (S29) and the OPs is in units of T_{c0} .

1. OPs in the two-pocket model at zero field, $E_Z = 0$

The purpose of this section is to elucidate the limitations on the parameters of the two-pocket model imposed by the zero field data (cf. inset of Figure S2), where the BCS ratio of the superconducting gap to the critical temperature is found. This implies that, in the case where there are two superconducting gaps, the larger one is measured in the experiment. In addition, in the experiment, quasiparticles tunnel into NbSe₂ mainly at the K/K' points, as this is where the energy gap is the smallest in the tunnel barrier material (few-layer WSe₂ or MoS₂)^{S26,S27}. In the previous work of some of us on bulk NbSe₂ with similar barriers, we found a negligible contribution from tunneling into the Γ point^{S28}. Therefore, we consider only tunneling into the K/K' points.

Specifically, we find that the BCS ratio of the superconducting gap to the critical temperature is achieved either when the Γ and K/K' pockets are decoupled or when the interaction amplitudes satisfy the following condition,

$$v^{\Gamma\Gamma} + 2v^{K\Gamma} = 2v^{KK} + v^{K\Gamma}. \quad (\text{S28})$$

The decoupled pockets are analyzed above, and here we consider the coupled pockets under the condition, (S28). This relation follows as the number of K pockets is twice as large than the number of Γ pockets. The relation (S28) is confirmed numerically in the Fig. S12. where the ratio of the gap Δ_s^K to the zero field critical temperature,

$$T_{c0}(v^{\beta\beta'}) = \frac{2\omega_D e^{\gamma_E}}{\pi} \exp\left(-\frac{v^{KK} + v^{\Gamma\Gamma}/2 + \sqrt{2(v^{K\Gamma})^2 + (v^{KK} - v^{\Gamma\Gamma}/2)^2}}{4N_0[(v^{K\Gamma})^2 - v^{\Gamma\Gamma}v^{KK}]}\right). \quad (\text{S29})$$

is shown as a function of $v^{\Gamma\Gamma}/v^{KK}$ and $v^{K\Gamma}/v^{KK}$. As the experimentally observed ratio is close to the BCS ratio, we restrict ourselves in the following to this line, which includes, in particular, the case where all interactions are equal.

2. The case of equal inter- and intra-pocket interactions

We now consider the case $v^{\Gamma\Gamma} = v^{KK} = v^{K\Gamma}$. In this section we show that this case is equivalent to a single pocket. It can be shown from the self consistency equations that in this case the OPs are equal $\Delta_s^K = \Delta_s^\Gamma = \Delta_s$, and the two self-consistency equations reduce to one:

$$\pi T \sum_{\omega_n} \left[\frac{\Delta_s}{|\omega_n|} - \left(\frac{2}{3} \langle f_0^K(\hat{\mathbf{k}}, \omega_n, \Delta_s) \rangle_{\varphi_{\mathbf{k}}} + \frac{1}{3} \langle f_0^\Gamma(\hat{\mathbf{k}}, \omega_n, \Delta_s) \rangle_{\varphi_{\mathbf{k}}} \right) \right] + \Delta_s \ln\left(\frac{T}{T_{c0}}\right) = 0, \quad (\text{S30})$$

where $f_0^{\Gamma(K)}(\hat{\mathbf{k}}, \omega_n, \Delta_s)$ are quasi-classical Green functions,^{S5}. That is, we effectively have a single pocket with field dependence which averages over the pair breaking effect at the K/K' and at Γ pockets.

The physical picture contained in Eq. (S30) is that of a single band, albeit anisotropic. For this reason, it has been possible to parametrize Eq. (S30) by the critical temperature, T_{c0} instead of the pairing amplitude λ . In general, this is not possible even close to T_{c0} ^{S29}. Furthermore, the pair breaking equation for the critical field reads,

$$\ln\left(\frac{T}{T_{c0}}\right) + \left(\frac{2}{3}\mathcal{S}_K + \frac{1}{3}\mathcal{S}_\Gamma\right) = 0, \quad (\text{S31})$$

where

$$\mathcal{S}_K = \pi T \sum_{\omega_n} \frac{1}{|\omega_n|} \left(\frac{E_Z^2}{E_Z^2 + (E_{SO}^K)^2 + \omega_n^2} \right), \quad \mathcal{S}_\Gamma = \pi T \sum_{\omega_n} \frac{1}{|\omega_n|} \left(\frac{E_Z^2}{\sqrt{(E_Z^2 + \omega_n^2) (E_Z^2 + (E_{SO}^\Gamma)^2 + \omega_n^2)}} \right). \quad (\text{S32})$$

The last equation can be obtained by linearizing Eq. (S30). Again, it evidently represents the average over the combined Fermi surface made out of K/K' and Γ pockets.

3. The effect of impurities on the OP

In the case where all the interactions amplitudes are equal, we saw that we effectively have a single band comprised of pairing in the K/K' and Γ pockets. Neglecting inter-valley scattering, the presence of impurities can effect the OP through the Γ pairing. This is because the spin-orbit nodes in the Γ pocket lead to the 'flattened' shape of the OP as a function of in-plane magnetic field at intermediate fields. (A model with two nodeless pockets cannot reproduce this aspect of the data.)

In order to include this effect, we write the Gorkov equation as

$$\left[i\omega_n \hat{\sigma}_0 - \hat{H}_{\text{BdG}}^\Gamma(\mathbf{k}) - \hat{\Sigma}^{(\Gamma)}(\omega_n) \right] \hat{G}^\Gamma(\mathbf{k}, \omega_n) = \hat{\sigma}_0 \quad (\text{S33})$$

where $\hat{\Sigma}^{(\Gamma)}(\omega_n)$ is the self-energy given withing the self-consistent Born approximation by^{S30}

$$\hat{\Sigma}^{(\Gamma)}(\omega_n) = \tau_\Gamma^{-1} \int \frac{d\varphi_{\mathbf{k}}}{2\pi} \int \frac{d\epsilon_{\mathbf{k}}^\Gamma}{\pi} \hat{\sigma}_z \hat{G}^\Gamma(\mathbf{k}; \omega_n) \hat{\sigma}_z, \quad (\text{S34})$$

where $\hat{\sigma}_z = \text{diag}(\sigma_0, -\sigma_0)$ and τ_Γ^{-1} is intra Γ pocket impurity scattering rate. We calculate the OP by finding the root of the self consistency (S30), where $f_0^\Gamma(\hat{\mathbf{k}}, \omega_n)$ now includes the effect of impurities as in Eq. (S33). In order to find the root we must evaluate $\langle f_0^\Gamma(\hat{\mathbf{k}}, \omega_n) \rangle_{\varphi_{\hat{\mathbf{k}}}}$ for any given Δ_s . This is done by calculating $\hat{\Sigma}^{(\Gamma)}(\omega_n, \Delta_s)$ for the given Δ_s by way of iterations using Eqs. (S33, S34), then inserting $\hat{\Sigma}^{(\Gamma)}(\omega_n, \Delta_s)$ into Eq. (S33) and finding $\langle f_0^\Gamma(\hat{\mathbf{k}}, \omega_n) \rangle_{\varphi_{\hat{\mathbf{k}}}}$. The results for different values of τ_Γ^{-1} are presented in Fig. S13. In our numerical calculations we take $E_{SO}^K/E_{SO}^\Gamma = 2.14$ based on Ref. S24 assuming that this ratio is roughly similar for mono- and bilayer systems.

Without disorder a reasonable fit to the experimental data is achieved (Figure S13). The level of experimental disorder is estimated to be at least ≈ 10 meV (cf. Section IC), which is to say tens of T_{cs} . The inclusion of such a strong disorder at the level of the self-consistent Born approximation makes the procedure numerically unstable. Nevertheless, even at the levels of disorder we are able to incorporate, it can already be seen that the fit becomes progressively worse with increasing disorder (Figure S13). At even higher values of disorder scattering rate, we expect it to continue to get worse compared to the one obtained with the triplet pairing. In addition, with increasing disorder, an increase in the value of spin-orbit coupling necessary to obtain the same critical field. Finally, at very strong levels of disorder, i.e. $1/\tau_\Gamma \gg \Delta_{SO}^\Gamma$, the Γ -pocket is described by AG-theory which yields a field-dependence of the OP inconsistent with the data.

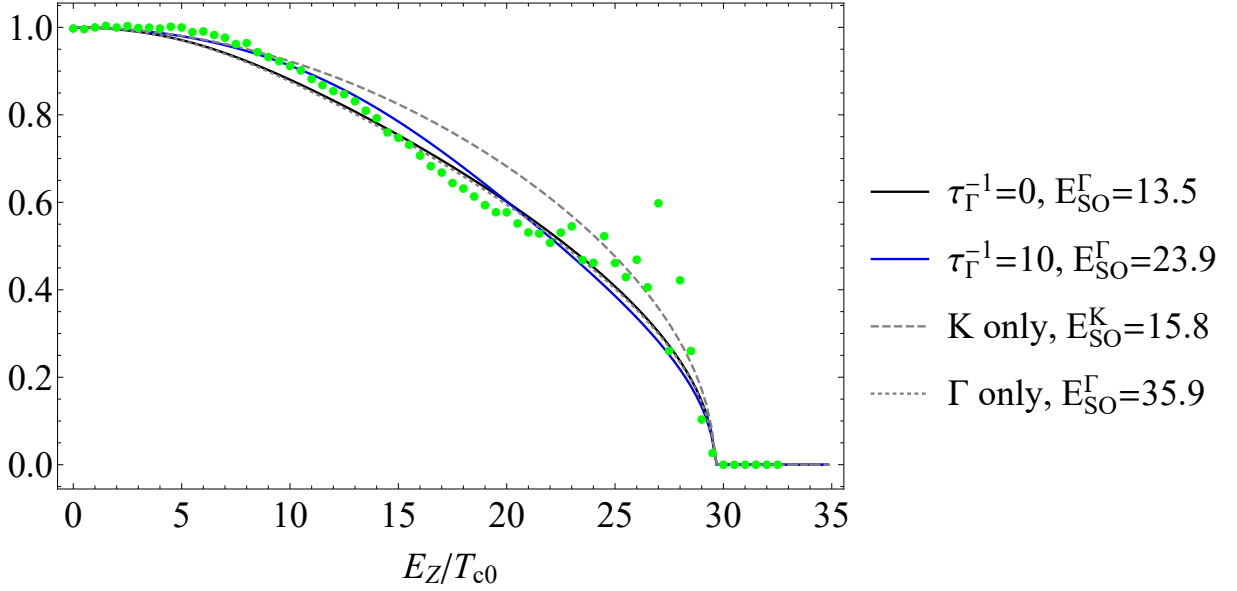


Figure S13 The OP as a function of E_Z . The black and blue lines have K and Γ equal pairing interactions and are calculated by numerically solving Eq. (S30) for the clean case (black line) and with a high impurity scattering rate of $\tau_{\Gamma}^{-1} = 10$ (blue line). The dashed and dotted lines show the OP in the clean case with only the K and Γ pocket pairings, respectively. These are found by replacing in Eq. (S30) f_0^{Γ} by f_0^K for the K pocket and replacing f_0^K with the f_0^{Γ} for the Γ pocket. The green dots show the experimental data and the SOC for each line is taken to fit the experimental critical field. The parameters τ_{Γ}^{-1} and $E_{SO}^{\Gamma}, E_{SO}^K$ are in units of T_{c0} and for the black and blue lines we take $E_{SO}^K/E_{SO}^{\Gamma} = 2.14$.

D. Two-pocket superconductivity in NbSe₂ - McMillan coupling

Here we address the possibility that multipocket physics, with a McMillan coupling^{S31} plays a significant role in our findings. As before we, consider the $K(K')$ and Γ pockets, originating from the Nb derived band^{S24}. Unlike in section II C where two-particle intra-pocket tunneling was discussed, the McMillan coupling considered here amounts to single-particle tunneling.

The theoretical model is presented in section IID 1, a comparison with experimental data is given in section IID 2, followed by a short discussion in section IID 3.

1. Multipocket model

We account for scattering within and between pockets by the following rates:

- τ^{-1} : scattering within the K, K' pockets (intravalley scattering). Note that this type of disorder has no effect on superconductivity due to the Anderson theorem,
- τ_{iv}^{-1} : Scattering between K and K' pockets (intervalley scattering),
- τ_{Γ}^{-1} : scattering within the Γ pocket,
- $\Gamma_{K\Gamma}, \Gamma_{\Gamma K}$: scattering from the K to the Γ pocket and vice-versa.

The following relation holds for inter-pocket scattering rates

$$\frac{\Gamma_{K\Gamma}}{\Gamma_{\Gamma K}} = \frac{N_{\Gamma}}{N_K}, \quad (\text{S35})$$

where N_K is the sum of the normal state DoS of the K and K' pockets, and N_{Γ} is the normal state DoS of the Γ pocket. Taking into account that DoS per pocket is approximately the same for K, K' and Γ , we have $N_K \approx 2N_{\Gamma}$ ^{S32}.

We will assume s -wave superconductivity, that originates from the K pocket, and is induced by the proximity effect in the Γ pocket through inter-pocket scattering. Furthermore, we will assume diffusive limit in the Γ pocket, $\tau_{\Gamma}^{-1} \gg E_{SO}^{\Gamma}, E_Z, \Delta_0, \Gamma_{ij}$. If the SOC is sufficiently strong in both pockets, that is, if $E_{SO}^K \gg \Delta_0, \Gamma_{ij}, E_Z, \tau_{iv}^{-1}$, and

$(E_{SO}^\Gamma)^2 \tau_\Gamma \gg \Delta_0, E_Z, \Gamma_{ij}$, the density of states is given by the Kaiser-Zuckermann formula^{S33}, which is a multiband extension of the Abrikosov-Gor'kov theory. Namely, depairing in both K and Γ pockets is captured by the rates quadratic in magnetic field

$$\Gamma_{AG}^K(E_Z) = \frac{E_Z^2}{(E_{SO}^K)^2 \tau_{iv}}, \quad \Gamma_{AG}^\Gamma(E_Z) = \frac{E_Z^2}{(E_{SO}^\Gamma)^2 \tau_\Gamma}, \quad (\text{S36})$$

and we can introduce the functions u_K and u_Γ that satisfy

$$\frac{\omega_n}{\Delta} = u_K - \frac{\Gamma_{AG}^K(E_Z)}{\Delta} \frac{u_K}{\sqrt{1+u_K^2}} + \frac{\Gamma_{K\Gamma}}{\Delta} \frac{u_K - u_\Gamma}{\sqrt{1+u_\Gamma^2}} = -\frac{\Gamma_{AG}^\Gamma(E_Z)}{\Delta} \frac{u_\Gamma}{\sqrt{1+u_\Gamma^2}} + \frac{\Gamma_{\Gamma K}}{\Delta} \frac{u_\Gamma - u_K}{\sqrt{1+u_K^2}}. \quad (\text{S37})$$

Here, Δ is the intrinsic gap from the K pocket. Then, the DoS in the superconducting state is given as

$$\nu(E) = \sum_{i=K,\Gamma} N_i \Re \left[\frac{u_i}{\sqrt{1+u_i^2}} \right]_{i\omega_n \rightarrow E}. \quad (\text{S38})$$

The intrinsic gap Δ satisfies the self-consistency condition

$$\Delta = 2\pi T N_K |v_s| \sum_{\omega_n > 0} \frac{1}{\sqrt{1+u_K^2}}. \quad (\text{S39})$$

An alternative formulation is given by Eq. (S40), parameterized in terms of the critical temperature T_c instead of the coupling constant v_s

$$\ln \left(\frac{T}{T_c} \right) + \frac{\Gamma_{K\Gamma}}{\Gamma_{K\Gamma} + \Gamma_{\Gamma K}} \left[\psi \left(\frac{1}{2} \right) - \psi \left(\frac{1}{2} + \frac{\Gamma_{K\Gamma} + \Gamma_{\Gamma K}}{2\pi T_c} \right) \right] = 2\pi T \sum_{\omega_n > 0} \left[\frac{1}{\Delta} \frac{1}{\sqrt{1+u_K^2}} - \frac{1}{\omega_n} \right]. \quad (\text{S40})$$

Here, $\psi(x)$ is the digamma function

Close to the phase transition to the normal state, that is, in the limit of vanishing Δ , it is possible to analytically evaluate Eq. (S39). The self-consistency condition then becomes

$$\ln \left(\frac{T}{T_c} \right) + \frac{\Gamma_{K\Gamma}}{\Gamma_{K\Gamma} + \Gamma_{\Gamma K}} \left[\psi \left(\frac{1}{2} \right) - \psi \left(\frac{1}{2} + \frac{\Gamma_{K\Gamma} + \Gamma_{\Gamma K}}{2\pi T_c} \right) \right] = \sum_{i=\pm} \frac{\alpha_i}{\chi^2} \left[\psi \left(\frac{1}{2} + \frac{\beta_i}{2\pi T} \right) - \psi \left(\frac{1}{2} \right) \right]. \quad (\text{S41})$$

Here T_c is the critical temperature. Furthermore, we have introduced

$$\begin{aligned} \chi &= \left(4\Gamma_{K\Gamma}\Gamma_{\Gamma K} + [\Gamma_{K\Gamma} - \Gamma_{\Gamma K} + \Gamma_{AG}^K(E_Z^c) - \Gamma_{AG}^\Gamma(E_Z^c)]^2 \right)^{1/2}, \\ \alpha_\pm &= \frac{1}{2} \left(-\chi^2 \pm \chi [\Gamma_{K\Gamma} - \Gamma_{\Gamma K} + \Gamma_{AG}^K(E_Z^c) - \Gamma_{AG}^\Gamma(E_Z^c)] \right), \\ \beta_\pm &= \frac{1}{2} \left(\Gamma_{K\Gamma} + \Gamma_{\Gamma K} + \Gamma_{AG}^K(E_Z^c) + \Gamma_{AG}^\Gamma(E_Z^c) \mp \chi \right), \end{aligned} \quad (\text{S42})$$

where E_Z^c is the upper critical field. Equation (S41) can be used to calculate the E_Z^c , provided that the scattering parameters are known.

2. Comparison with the experiment

The main goal is to obtain the $\Delta(H)$ dependence, based on equation (S40). As it stands there are five parameters: the critical temperature T_c , the scattering rates $\Gamma_{K\Gamma}$ and $\Gamma_{\Gamma K}$, and the Abrikosov-Gorkov depairing parameters Γ_{AG}^K and Γ_{AG}^Γ . In order to reduce the size of the parameter space, and to ease the exploration, some physically motivated constraints were placed on the parameter values.

a. Zero magnetic field

At zero field the Abrikosov-Gorkov parameters do not play a role and the order parameter is a function of $\Delta = \Delta(T, T_c, \Gamma_{K\Gamma}, \Gamma_{\Gamma K})$. The temperature was fixed to the experimental one ($T = 1.3\text{K}$) and the ratio of the pocket scattering rates is set according to Eq. (S35): $\Gamma_{\Gamma K} = 2\Gamma_{K\Gamma}$.

With this, at $H = 0$ it remains to determine T_c , this was done by constraining the value of Δ to $\approx 390\mu\text{eV}$, as obtained in the experiment (cf. inset of Figure S2). Then we can solve for T_c as a function of $\Gamma_{K\Gamma}$. The result is shown on figure S14: at zero coupling the ratio $\frac{\Delta}{k_B T_c}$ starts from the BCS value of ≈ 1.76 and grows as the coupling is increased. Therefore for the same value of Δ the critical temperature of a multipocket superconductor is lower than that of a BCS one. The densities of states of both pockets, at $H = 0$, for select values of $\Gamma_{K\Gamma}$ are shown in figures S15 and S16.

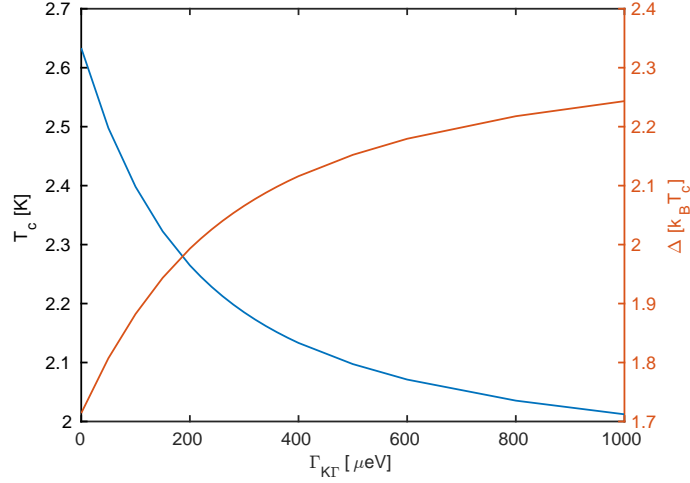


Figure S14 The dependence of T_c on $\Gamma_{K\Gamma}$, constrained to $\Delta \approx 390\mu\text{eV}$ at $T = 1.25\text{K}$.

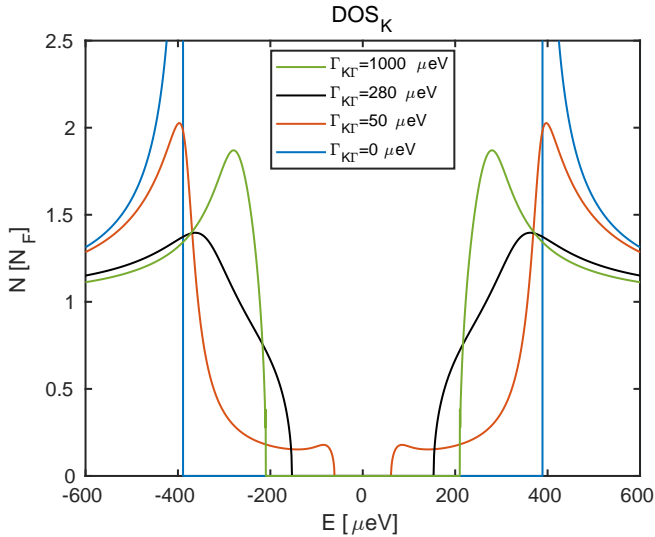


Figure S15 The DOS in the K pocket vs $\Gamma_{K\Gamma}$.

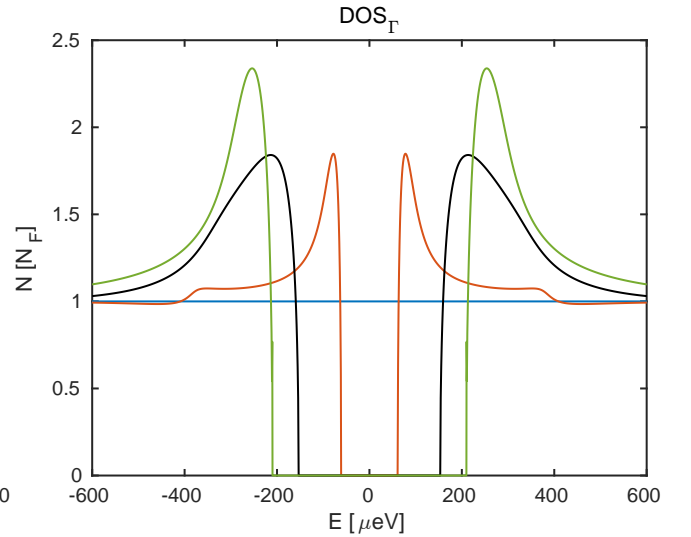


Figure S16 The DOS in the Γ pocket vs $\Gamma_{K\Gamma}$.

b. Finite magnetic field

At finite fields the values of the depairing parameters in both pockets play a significant role. Here they are parametrized as $\Gamma_{AG}^K(H) = \Gamma_{AG}^K H^2$ and $\Gamma_{AG}^\Gamma(H) = \Gamma_{AG}^\Gamma H^2$. Equation (S41) can be used to determine the values of Γ_{AG}^K and Γ_{AG}^Γ such that the critical field matches the experimentally determined one $H_c = 30\text{T}$. No matter what the inter-pocket coupling is, a solution will always exist where $\Gamma_{AG}^\Gamma = 0$ and $\Gamma_{AG}^K = \Gamma_c^{AG}(\Gamma_{K\Gamma})$, which satisfies the H_c

constraint. At zero coupling this is the only solution. Figure S17 shows Γ_{AG}^Γ vs Γ_{AG}^K , for different coupling strengths. Above a certain coupling strength the experimental H_c can be reproduced by depairing in either pocket, but below this threshold $H_c = 30\text{T}$ can be obtained only with a non-zero value of Γ_{AG}^K .

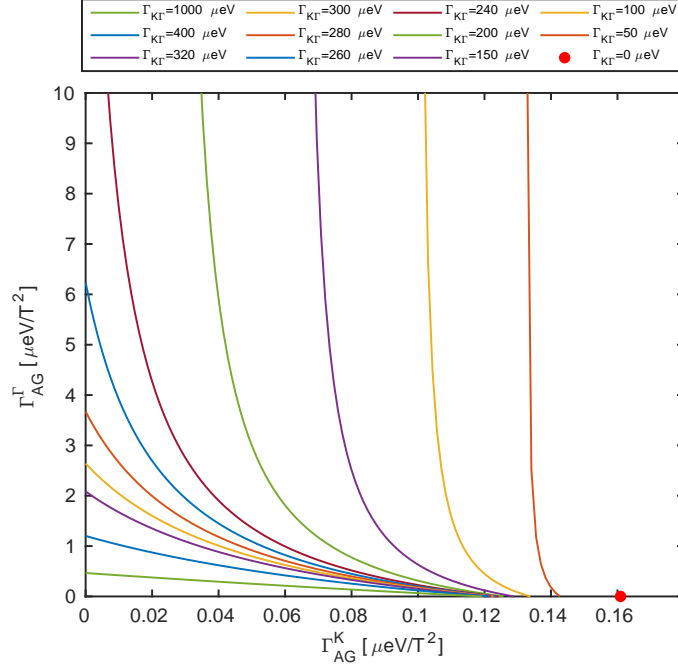


Figure S17 The values of Γ_{AG}^K and Γ_{AG}^Γ which result in $H_c = 30\text{T}$, for several values of $\Gamma_{K\Gamma}$ ($T = 1.25\text{K}$).

Consequently, the parameter space can be reduced to just two parameters: $\Gamma_{K\Gamma}$ and Γ_{AG}^K . We can now proceed and compare the $\Delta(H)$ curves with the experimental one.

In either the limit of zero coupling or very high coupling ($\Gamma_{K\Gamma} \gg \Delta$) the field dependence reduces to the Abrikosov-Gorkov one. This makes sense, as at high couplings the bands are indistinguishable (i.e. DOS in both pockets is the same - the green traces in figures S15 and S16), so depairing in either pocket can kill superconductivity, and therefore leads to the same $\Delta(H)$ trace. Figures S18 and S19 show the zero coupling case (i.e. AG dependence) and the highly coupled one (for several combinations of $(\Gamma_{AG}^K, \Gamma_{AG}^\Gamma)$, which all overlap) respectively.

Next, the case of intermediate coupling will be discussed, for several values of $\Gamma_{K\Gamma}$, and compared with our experimental data.

Figure S20 shows $\Delta(H)$ for $\Gamma_{K\Gamma} = 260\mu\text{eV}$: The traces for which the depairing is dominantly in the K pocket (e.g. the blue trace) agree with the data close to $H = 0$ and $H = H_c$, but not in between. If the depairing is only in the Γ pocket the trace lies below the experimental data for all fields. The purple trace shows the highest value of Γ_G which still fits the low and high field data, increasing it further will improve the fit at intermediate fields, but at the expense of the former two.

Figure S21 shows $\Delta(H)$ for $\Gamma_{K\Gamma} = 280\mu\text{eV}$: The green trace, for which the depairing is solely in the Γ pocket, reproduces the experimental data relatively well, except for the bump visible at $H > 20\text{T}$. The "revival" of superconductivity, relative to the previous case, can be understood in the following way - the pockets are coupled strongly, superconductivity originates in the K pocket while the depairing is induced in the Γ pocket, and a smaller depairing strength is needed to obtain the same critical field. Lower depairing rates in Γ (and higher in K) all result in traces above the experimental data.

Figure S22 shows $\Delta(H)$ for $\Gamma_{K\Gamma} = 300\mu\text{eV}$: The same qualitative behavior is observed as for $\Gamma_{K\Gamma} = 280\mu\text{eV}$, but with a slightly worse agreement at intermediate fields. Figure S23 shows $\Delta(H)$ for $\Gamma_{K\Gamma} = 320\mu\text{eV}$: all $\Delta(H)$ curves now lie above the experimental data.

We conclude that if the two pocket model is to explain the experimental $\Delta(H)$ curve the appropriate scattering rate is close to $\Gamma_{K\Gamma} \approx 280\mu\text{eV}$.

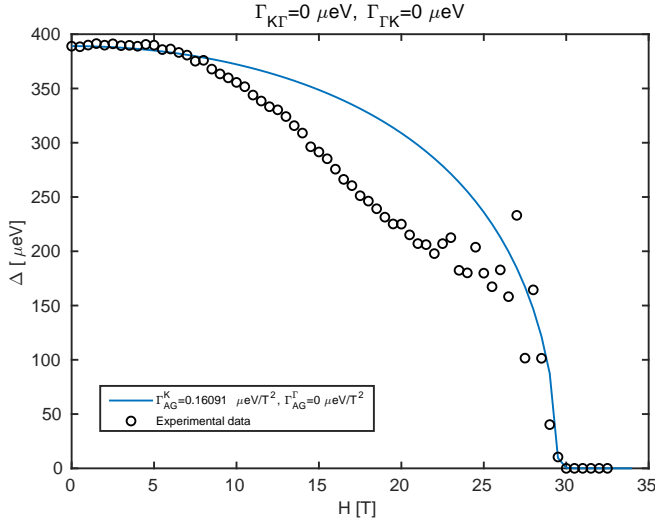


Figure S18 Δ vs H curve for uncoupled pockets. The depairing is in the K pocket.

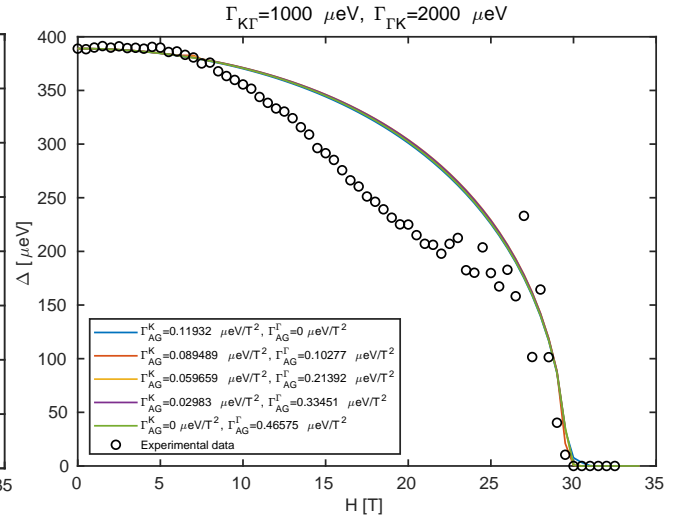


Figure S19 Δ vs H curve for highly coupled pockets. The depairing is either in the K pocket (blue line), the Γ pocket (green line), or both (other lines).

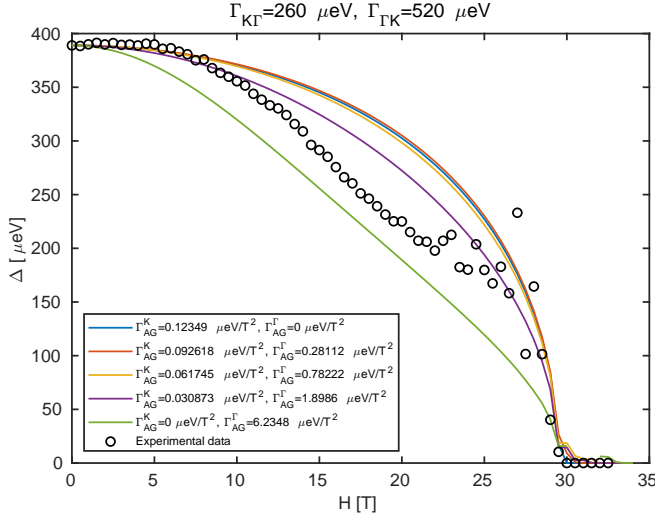


Figure S20 Δ vs H curve for $\Gamma_{K\Gamma} = 260\mu\text{eV}$ and $\Gamma_{\Gamma K} = 520\mu\text{eV}$.

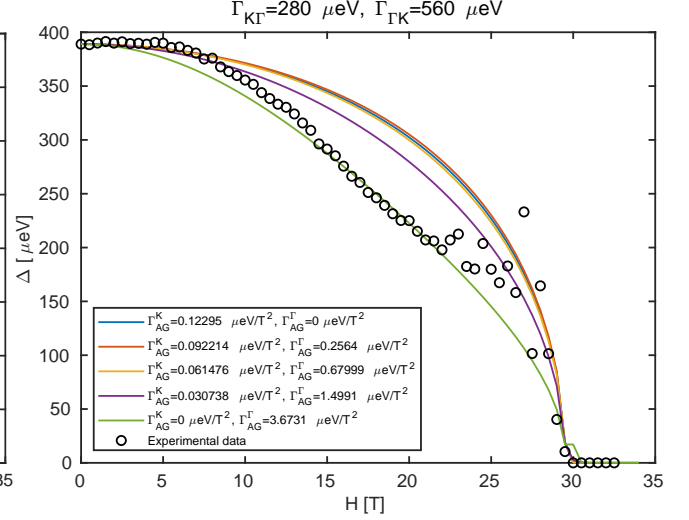


Figure S21 Δ vs H curve for $\Gamma_{K\Gamma} = 280\mu\text{eV}$ and $\Gamma_{\Gamma K} = 560\mu\text{eV}$.

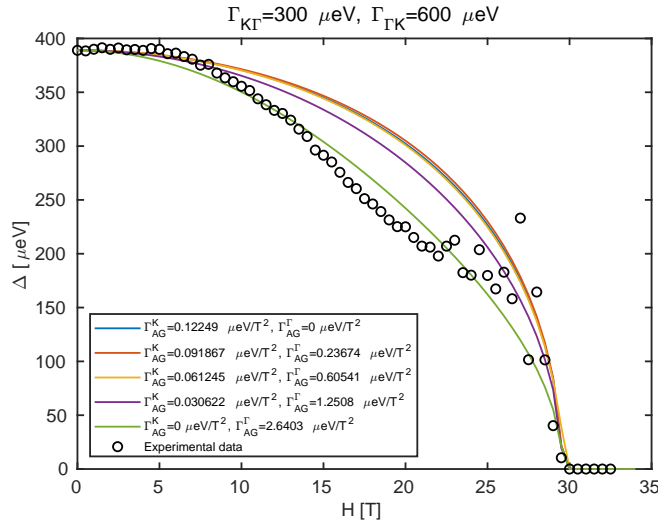


Figure S22 Δ vs H curve for $\Gamma_{K\Gamma} = 300\mu\text{eV}$ and $\Gamma_{\Gamma K} = 600\mu\text{eV}$.

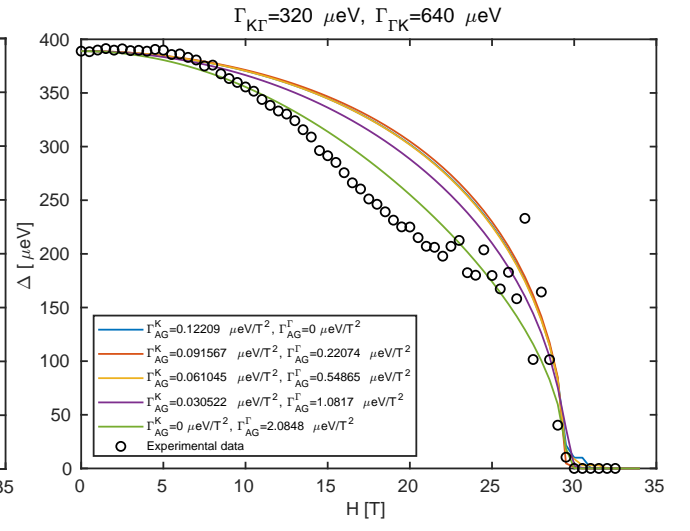


Figure S23 Δ vs H curve for $\Gamma_{K\Gamma} = 320\mu\text{eV}$ and $\Gamma_{\Gamma K} = 640\mu\text{eV}$.

3. Comments and discussion

Based on the analysis presented in this section, a McMillan two-pocket model can, in principle, reproduce the $\Delta(H)$ curve measured in this work, with a large inter-pocket coupling. For the $K\Gamma$ coupling strength required to explain the $\Delta(H)$ data the DOS of the K pocket, which is dominantly probed in tunneling experiments^{S26,S27}, is given by the black trace in figure S15. The coherence peak reaches up to $\approx 1.4N_F$, which is comparable to our spectra measured at a finite temperature and with additional broadening, both of which reduce the height of the observed coherence peak. The shoulder, which is clearly present in the theoretical DOS, is absent from tunneling data measured with high-quality junctions - see figure 2c of the main text as well as the bi-layer tunneling spectrum from^{S2}, reproduced here in figure S8.

Additionally, in thin samples we observe the BCS ratio of $\Delta/T_c \approx 1.76$ (c.f. fig. S2), while for the coupling needed to fit the $\Delta(H)$ curve the ratio is ≈ 2.1 (c.f. fig S14).

Thus, based on spectroscopic and transport data, we argue that the two pocket model with a type McMillan coupling^{S31} is an unlikely explanation of the observed data.

References

-
- * These two authors contributed equally
- [S1] Dvir, T. et al. Spectroscopy of bulk and few-layer superconducting nbse2 with van der waals tunnel junctions. *Nature communications* **9**, 1–6 (2018).
- [S2] Khestanova, E. et al. Unusual suppression of the superconducting energy gap and critical temperature in atomically thin nbse2. *Nano letters* **18**, 2623–2629 (2018).
- [S3] Dvir, T. et al. Spectroscopy of bulk and few-layer superconducting nbse 2 with van der waals tunnel junctions. *Nature communications* **9**, 1–6 (2018).
- [S4] Tsen, A. W. et al. Nature of the quantum metal in a two-dimensional crystalline superconductor. *Nature Physics* **12**, 208–212 (2016). URL <https://www.nature.com/articles/nphys3579>.
- [S5] Haim, M., Mockli, D. & Khodas, M. Signatures of triplet correlations in density of states of ising superconductors. *Phys. Rev. B* **102**, 214513 (2020). URL <https://link.aps.org/doi/10.1103/PhysRevB.102.214513>.
- [S6] Skalski, S., Betbeder-Matibet, O. & Weiss, P. Properties of superconducting alloys containing paramagnetic impurities. *Physical Review* **136**, A1500 (1964).
- [S7] Dynes, R., Narayanamurti, V. & Garno, J. P. Direct measurement of quasiparticle-lifetime broadening in a strong-coupled superconductor. *Physical Review Letters* **41**, 1509 (1978).
- [S8] Abrikosov, A. & Gor'kov, L. Zh. é ksp. teor. fiz. 39, 1781 1960 sov. phys. *JETP* **12**, 1243 (1961).
- [S9] Herman, F. & Hlubina, R. Microscopic interpretation of the dynes formula for the tunneling density of states. *Physical Review B* **94**, 144508 (2016).
- [S10] Hörhold, S., Graf, J., Marganska, M. & Grifoni, M. Two bands Ising superconductivity from Coulomb interactions in monolayer NbSe₂. *2S* (2022). URL <http://arxiv.org/abs/2206.06645>. ArXiv:2206.06645.
- [S11] Fischer, M. H., Sigrist, M. & Agterberg, D. F. Superconductivity without inversion and time-reversal symmetries. *Phys. Rev. Lett.* **121**, 157003 (2018). URL <https://link.aps.org/doi/10.1103/PhysRevLett.121.157003>.
- [S12] Hlobil, P., Jandke, J., Wulflhekel, W. & Schmalian, J. Tracing the Electronic Pairing Glue in Unconventional Superconductors via Inelastic Scanning Tunneling Spectroscopy. *Physical Review Letters* **118**, 167001 (2017). URL <https://link.aps.org/doi/10.1103/PhysRevLett.118.167001>. Publisher: American Physical Society.
- [S13] Reed, M. A. Inelastic electron tunneling spectroscopy. *Materials Today* **11**, 46–50 (2008). URL <https://www.sciencedirect.com/science/article/pii/S1369702108702384>.
- [S14] Littlewood, P. B. & Varma, C. M. Amplitude collective modes in superconductors and their coupling to charge-density waves. *Physical Review B* **26**, 4883–4893 (1982). URL <https://link.aps.org/doi/10.1103/PhysRevB.26.4883>. Publisher: American Physical Society.
- [S15] Ilić, S., Meyer, J. S. & Houzet, M. Enhancement of the Upper Critical Field in Disordered Transition Metal Dichalcogenide Monolayers. *Physical Review Letters* **119**, 117001 (2017). URL <https://link.aps.org/doi/10.1103/PhysRevLett.119.117001>. Publisher: American Physical Society.
- [S16] de la Barrera, S. C. et al. Tuning Ising superconductivity with layer and spin-orbit coupling in two-dimensional transition-metal dichalcogenides. *Nature Communications* **9**, 1427 (2018). URL <https://www.nature.com/articles/s41467-018-03888-4>.
- [S17] Möckli, D. & Khodas, M. Magnetic-field induced s + if pairing in Ising superconductors. *Physical Review B* **99**, 180505(R) (2019). URL <https://link.aps.org/doi/10.1103/PhysRevB.99.180505>.
- [S18] Ilic, S., Meyer, J. S. & Houzet, M. Title. In preparation.

- [S19] Tang, B. G., Bruder, C. & Belzig, W. Preprint, 2011.07080.
- [S20] Möckli, D. & Khodas, M. Ising superconductors: Interplay of magnetic field, triplet channels, and disorder. *Phys. Rev. B* **101**, 014510 (2020). URL <https://link.aps.org/doi/10.1103/PhysRevB.101.014510>.
- [S21] Maki, K. & Tsuneto, T. Pauli Paramagnetism and Superconducting State. *Progress of Theoretical Physics* **31**, 945–956 (1964). URL <https://academic.oup.com/ptp/article-lookup/doi/10.1143/PTP.31.945>.
- [S22] Abrikosov, A. A. & Gor'kov, L. P. *Soviet Physics JETP* **12**, 1243–1253 (1961).
- [S23] Noat, Y. et al. Quasiparticle spectra of 2 h- nbse 2: Two-band superconductivity and the role of tunneling selectivity. *Physical Review B* **92**, 134510 (2015).
- [S24] Wickramaratne, D., Khmelevskiy, S., Agterberg, D. F. & Mazin, I. Ising superconductivity and magnetism in nbse 2. *Physical Review X* **10**, 041003 (2020).
- [S25] Suhl, H., Matthias, B. T. & Walker, L. R. Bardeen-cooper-schrieffer theory of superconductivity in the case of overlapping bands. *Phys. Rev. Lett.* **3**, 552–554 (1959). URL <https://link.aps.org/doi/10.1103/PhysRevLett.3.552>.
- [S26] Zhu, Z. Y., Cheng, Y. C. & Schwingenschlögl, U. Giant spin-orbit-induced spin splitting in two-dimensional transition-metal dichalcogenide semiconductors. *Physical Review B* **84**, 153402 (2011). URL <https://link.aps.org/doi/10.1103/PhysRevB.84.153402>. Publisher: American Physical Society.
- [S27] Wang, Q. H., Kalantar-Zadeh, K., Kis, A., Coleman, J. N. & Strano, M. S. Electronics and optoelectronics of two-dimensional transition metal dichalcogenides. *Nature Nanotechnology* **7**, 699–712 (2012). URL <https://doi.org/10.1038/nnano.2012.193>.
- [S28] Dvir, T. et al. Spectroscopy of bulk and few-layer superconducting NbSe2 with van der Waals tunnel junctions. *Nature Communications* **9**, 598 (2018). URL <http://www.nature.com/articles/s41467-018-03000-w>.
- [S29] Kogan, V. G. & Schmalian, J. Ginzburg-landau theory of two-band superconductors: Absence of type-1.5 superconductivity. *Phys. Rev. B* **83**, 054515 (2011). URL <https://link.aps.org/doi/10.1103/PhysRevB.83.054515>.
- [S30] Wickramaratne, D., Haim, M., Khodas, M. & Mazin, I. I. Magnetism-driven unconventional effects in ising superconductors: Role of proximity, tunneling, and nematicity. *Phys. Rev. B* **104**, L060501 (2021). URL <https://link.aps.org/doi/10.1103/PhysRevB.104.L060501>.
- [S31] McMillan, W. L. Tunneling Model of the Superconducting Proximity Effect. *Physical Review* **175**, 537–542 (1968). URL <https://link.aps.org/doi/10.1103/PhysRev.175.537>. Publisher: American Physical Society.
- [S32] Sticlet, D. & Morari, C. Topological superconductivity from magnetic impurities on monolayer nbse 2. *Physical Review B* **100**, 075420 (2019).
- [S33] Kaiser, A. & Zuckermann, M. Mcmillan model of the superconducting proximity effect for dilute magnetic alloys. *Physical Review B* **1**, 229 (1970).